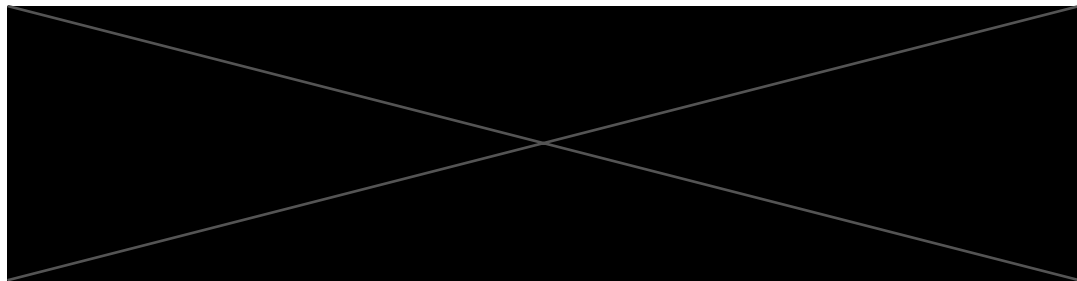




UNIVERSITY OF
CAMBRIDGE
Department of Engineering

Joint Space Mapping of the Lower Limbs in Clinical CT

Author Name: Abdullah M. Athar
Supervisor: Dr Andrew Gee
Date: June 2, 2021



Joint Space Mapping of the Lower Limbs in Clinical CT

Abdullah M. Athar - Sidney Sussex College

Technical Abstract

This project is motivated by Osteoarthritis (OA) of the hip, a widespread health problem that causes morbidity in the older population and is currently mainly treated through joint replacement. While earlier studies have focused on 2D radiographs for characterising OA, 3D CT based methodologies have recently gained traction for identifying risk factors and detecting therapeutic successes of treatments for the disease. The project builds on research relating to Joint Space Mapping (JSM), a novel CT-based 3D imaging analysis technique that delivers joint space width (JSW) maps of human joints. This technique has been developed to further improve the diagnostic and therapeutic successes seen with structural joint disease via the limited capabilities of 2D methodologies.

Most retrospective analyses of joint space maps assume measurement noise in the prospectively collected CT data due to uncontrolled joint positioning. The focus of this investigation is on the effect of inconsistent hip positioning on the output of JSM. In particular, this project is concerned with quantifying the change in the 3D JSW delivered by JSM as a function of hip rotation to understand the tolerance of the technique to variability in joint positioning. Previous studies on JSM concerned with its technical validation, applications and feasibility use CT data without any position standardisation, and the sensitivity analysis that this project carries out should enhance confidence in the results of all such studies.

This report investigates a study cohort of 101 individuals with repeated CT scans of their hip joints. Patient positioning was not controlled during the scans. The investigation is presented in three main stages. Firstly, a suitable quantification of the hip rotation was carried out. The joint space width profiles were then obtained for each hip, and spatial normalisation was carried out. Finally, the absolute change in 3D JSW between baseline and follow-up hips was investigated against the magnitude of hip rotation between scans using Statistical Parametric Mapping (SPM).

The report begins by outlining the process of suitably quantifying the hip joint rotation. A semi-automated method of finding the rotation, using triangulated meshes to represent the pelvis and proximal femur, was developed. This involved extracting the 3D femoral and pelvic surfaces from the CT data using *Stradview*, a software designed for CT data visualisation and manipulation. A pelvic statistical shape model (SSM) was developed to expedite the 3D surface extraction process due to the large size of the study cohort. Once all patient hip joints were extracted as 3D mesh objects, a coordinate system was defined on the pelvis and the proximal femur, and the rotation

matrix between the two was evaluated. A simple method to find the absolute angle of rotation between each patient's baseline and follow-up hips is also presented.

Furthermore, an expert radiologist performed JSM on all hips and provided the joint space width data mapped on each subject's acetabular surface for this investigation. The report details the process of spatial normalisation, which is necessary for statistical analyses using SPM. This involved transferring JSW data from each individual's acetabular surface onto a canonical acetabular surface. Spatial normalisation ensured that the JSW data from every individual could be analysed in a standard anatomical space, allowing comparisons across subjects with varied joint space profiles.

The report details the results of the statistical tests to investigate the effect of hip rotation on the error, measured as the absolute JSW difference, between baseline and follow-up scans. Visualisation of this error, averaged across the cohort, on the canonical acetabular surface revealed regions of high magnitude at the joint margin. However, SPM showed no significant regional effects of hip rotation. Additionally, cohort stratification into two groups based on the magnitude of hip rotation was carried out. Although non-significant, the error was visibly higher around the joint margin for the group with larger hip rotation. A further hypothesis that the joint space narrows between baseline and follow-up scans was also investigated. However, no significant evidence of joint narrowing was found via SPM when the time between the scans was incorporated in the statistical analysis.

Additionally, a scalar average of the 3D absolute JSW difference was investigated against hip rotation. The statistical analysis revealed no significant relationship between the two quantities. This indicated that hip rotation was not a significant source of measurement error in JSM, which delivered an average precision of ~ 0.3 mm between baseline and follow-up joint space widths.

After evaluating the gradient of the cohort average JSW across the joint, it was found that regions of high gradient corresponded with regions of high error between baseline and follow-up hips. The error was highest around the outer joint edges, indicating that it may be caused by an operator bias in the segmentation of the joint space patches. Finally, two approaches to minimise the segmentation error were investigated, and their performance was evaluated.

In addition to carrying out a sensitivity analysis of JSM on hip rotation, this project proposes a technique for identifying the 3D femoral neck axis. This could be used in conjunction with the semi-automated hip angulation protocol to output clinically-relevant hip rotations. The advantages of this semi-automated approach over manual clinical practices are also discussed. A further successful outcome of this project is the development of a statistical shape model of the human pelvis, which has practical applications in surgical planning.

Contents

List of abbreviations	2
1 Introduction	3
1.1 Motivation	3
1.2 Techniques for Osteoarthritis Characterisation	3
1.3 Joint Space Mapping (JSM)	5
1.3.1 Preparation of the Joint Space Patch	5
1.3.2 3D Joint Space Data Sampling	6
1.3.3 Success of Joint Space Mapping	7
1.3.4 Knowledge Gaps in the Study of JSM	10
2 Theory and Design of Experiment	11
2.1 Patient Demographics	11
2.2 CT Data	12
2.3 Mesh Representation of the Hip Joint	13
2.4 Method Overview	14
3 Statistical Shape Modelling	15
3.1 Motivation - 3D Surface Extraction	15
3.2 Segmentation of the Pelvis in <i>Stradview</i>	16
3.3 Defining a Canonical Hemipelvis	17
3.4 Building a Statistical Shape Model Using <i>wxRegSurf</i>	18
3.5 3D Surface Representation of the Femur	20
4 Coordinate System Definitions	21
4.1 Use of Anatomical Landmarks	21
4.2 Pelvis Coordinate System	21
4.3 Femur Coordinate System	22
4.3.1 Femoral Neck Axis	22
4.3.2 3D Femoral Coordinate System	23
5 Finding the Hip Joint Angle	24
5.1 Finding Clinically-Relevant Joint Rotation	24
5.2 Hip Angulation as Composed of Elemental Rotations	25

6 Statistical Parametric Mapping (SPM)	27
7 Results and Discussion	29
7.1 Femoral Neck Axis Definition	29
7.2 Comparison of Manual and Semi-automated Angles	30
7.3 Effect of Hip Angulation on JSM Output	32
7.4 Dependence of Average JSW on Hip Rotation	35
7.5 Intra-operator Variability of Angle Measurement	36
7.6 Analysis of Joint Space Maps	37
7.7 Stratification of Data	41
7.8 Reproducibility Bias of JSM	43
7.9 Limitations	44
8 Summary and Recommendations for Further Study	45
8.1 Conclusions	45
8.2 Recommendation for Future Work	45
A Impact of COVID-19	47
B Risk assessment retrospective	47

List of abbreviations

JSM	Joint Space Mapping
JSW	Joint space width
CT	Computed tomography
HU	Hounsfield unit
MPR	Multiplanar reformatting
CUED	Cambridge University Engineering Department
LAD	Locally affine deformation
SSM	Statistical shape model
SPM	Statistical Parametric Mapping
OA	Osteoarthritis
OARSI-OMERACT	Osteoarthritis Research Society International–Outcome Measures in Rheumatology
ICP	Iterative closest point
HRpQCT	High-resolution peripheral quantitative computed tomography

Acknowledgements

I would like to thank Dr Andrew Gee for his continuous support throughout this project, in the form of supervisions, encouragement and prompt responses to queries. His experience, ideas and insights were invaluable to this project.

I would also like to thank Dr Tom Turmezei for providing the clinical dataset and joint space maps for this project. His support and clinical insights were pivotal to the successful completion of the project.

1 Introduction

1.1 Motivation

Osteoarthritis (OA) is a common joint disorder affecting the global population, especially causing morbidity in the elderly. In its early stages, the disease manifests as loss of cartilage around the joint, resulting in a narrowing of the joint space. This is temporally followed by sclerosis of the underlying bone and osteophyte formation (Felson 1988).

Earlier studies have focused on 2D radiographs as the gold standard for the characterisation of osteoarthritis. Recently, there has been a shift in ideology towards using 3D CT data to understand the disease morphology and progression better. Turmezei et al. (2018) have devised a novel 3D technique, Joint Space Mapping (JSM), based on the premise that 3D modelling would yield more useful information about the joint space phenotype and disease.

The need for consistent joint positioning when acquiring joint space width values with this novel technique has not been investigated before. This may limit the amount of retrospective analysis that could be carried out on available CT datasets wherein the hip joint positioning was not normalised during CT acquisition. Moreover, it is hard to perfectly neutralise the patient's position, and the robustness of JSM to this intrinsic variability in the acquisition of CT data needs to be investigated. This project analyses the sensitivity of the 3D JSM method to the hip joint angle. We quantify the misalignment relative to the perfectly neutral patient position, beyond which the technique outputs statistically different joint space width values. This misalignment can be decomposed into three principal modes of hip joint rotation, depicted in Figure 1.

1.2 Techniques for Osteoarthritis Characterisation

Earlier studies regarding OA have focused on 2D radiographs to investigate the disease, with different criteria for disease discussed in various studies. The variability in these criteria used to characterise OA affects the study results in different ways.

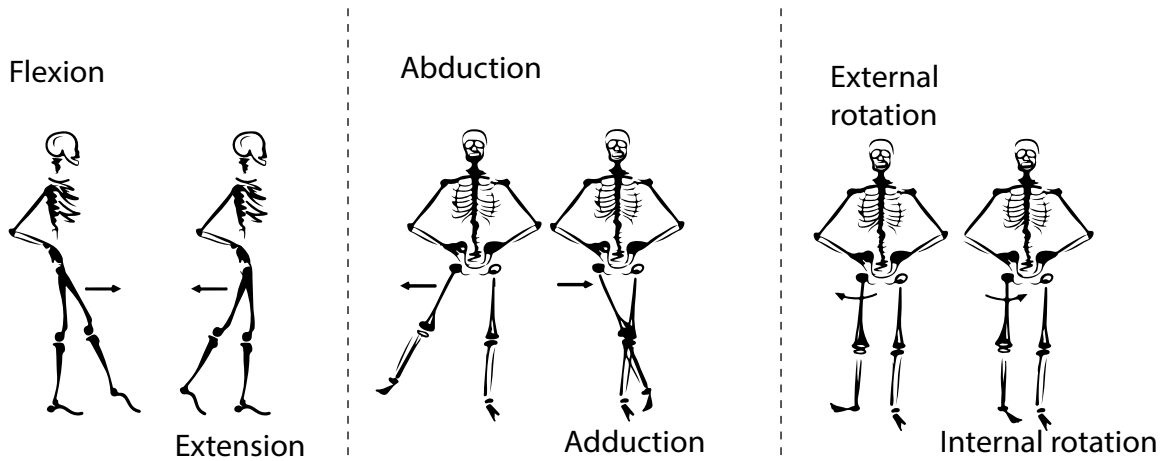


Figure 1: Principal modes of rotation of the hip joint ¹.

1. Clinical and epidemiological studies define disease with radiographic Kellgren and Lawrence (KL) grading (Kellgren et al. 1957), wherein the disease is graded from zero to four. This subjective, semi-quantitative grading has been shown to suffer from multiple varied definitions and problematic reliability (Turmezei et al. 2014). This has resulted in varying conclusions about the severity and presence of disease, especially in group studies, so that in certain joints, one observer may read four times as much definite osteoarthritis as another (Kellgren et al. 1957).
2. Some studies use no explicit radiographic criteria and rely on visual cues such as the Ahlbäck Criteria (Murray-Leslie et al. 1977; Lindberg et al. 1987), where the disease is only present if there is joint space narrowing.
3. The Osteoarthritis Research Society International (OARSI-OMERACT) suggest manually measuring the joint space width (JSW) to characterise OA as a narrowing of the joint. This recommendation is also the current gold standard for clinical trial imaging end points set by the FDA (Ornetti et al. 2009; Hunter et al. 2015).

Two important and unmet challenges in osteoarthritis imaging are the detection of early disease and an accurate prognosis. It is key to identify valid imaging biomarkers that reflect clinically relevant changes in disease. These can then be used to monitor the efficacy of new therapies in a trial setting and predict individuals at risk of new or rapidly progressing disease. Radiography and MRI have been the techniques most widely applied to hip osteoarthritis. However, there is a balance between MRI and radiographic evaluation capabilities regarding what features they can visualise and how sensitively they do it (Turmezei et al. 2014). Recognising that therapeutic trials

¹ Adapted <https://www.peninsulachiropractic.ca/blog/2018/07/09/hip-flexors-strong-glutes>

are in need of reliable biomarkers for optimising the chance of successful outcomes and that no single imaging biomarker has proved outstanding, Turmezei et al. (2018) have introduced Joint Space Mapping (JSM) to analyse the joint space and characterise OA. The details of this technique have been covered in Turmezei et al. (2018) and Turmezei et al. (2020), but since they are critical to this project, this report will discuss them briefly in Section 1.3.

1.3 Joint Space Mapping (JSM)

Turmezei et al. (2018) have proposed a new CT based semi-automatic imaging technique, JSM, which outputs 3D joint space maps of various joints in the human body. This technique strives to improve the diagnostic and therapeutic successes so far with structural joint disease, limited currently by operator-dependence and bias in radiograph analysis and disease characterisation by joint space width measurement. The study has demonstrated technical validation and inter-operator reproducibility of JSM. The technique uses CT data because of its efficient manipulation in reconstructing data volumes. The benefit of using CT data is that it is easy to visualise in 3D by CT data manipulation in designated software, such as *Stradview*². The JSM pipeline can be decomposed into two stages: preparing the "joint space patch" and sampling 3D joint space data onto this patch. These will be addressed in some detail next.

1.3.1 Preparation of the Joint Space Patch

As depicted in Figure 2, axial CT data is used to carry out femur segmentation. The CT data has standard clinical acquisition parameters: a reconstructed slice thickness of 1.5 mm, 0.31×0.31 mm pixel spacing and a smooth post-processing reconstruction kernel (Turmezei et al. 2016). Segmentation can either be carried out manually by drawing contours around relevant parts of the bone in the CT frames or using the model fitting functionality of *Stradview*. This attempts to minimise an error function based on the goodness of fit between a template femur mesh and the noisy CT data. Once a sufficient fit is achieved, contours from the fitted mesh can be mapped back onto the CT frames. The obtained contours are converted into a triangulated mesh, via a regularised marching tetrahedra algorithm (Treece et al. 1998), which can then be used to represent the 3D surface of the proximal femur.

Next, the shadow of the acetabulum is projected back onto the 3D femoral surface. This is done by drawing normals at each vertex in the proximal femur mesh and sampling the highest CT data value in Hounsfield units (HU) within 5 – 7 mm along the normal. The shadow of the acetabulum appears as a bright patch, the joint space patch, on the proximal femur surface, and can be separated and saved for the next step in the JSM pipeline. 3D multiplanar reformatting (MPR) is used to

²<https://mi.eng.cam.ac.uk/Main/StradView>

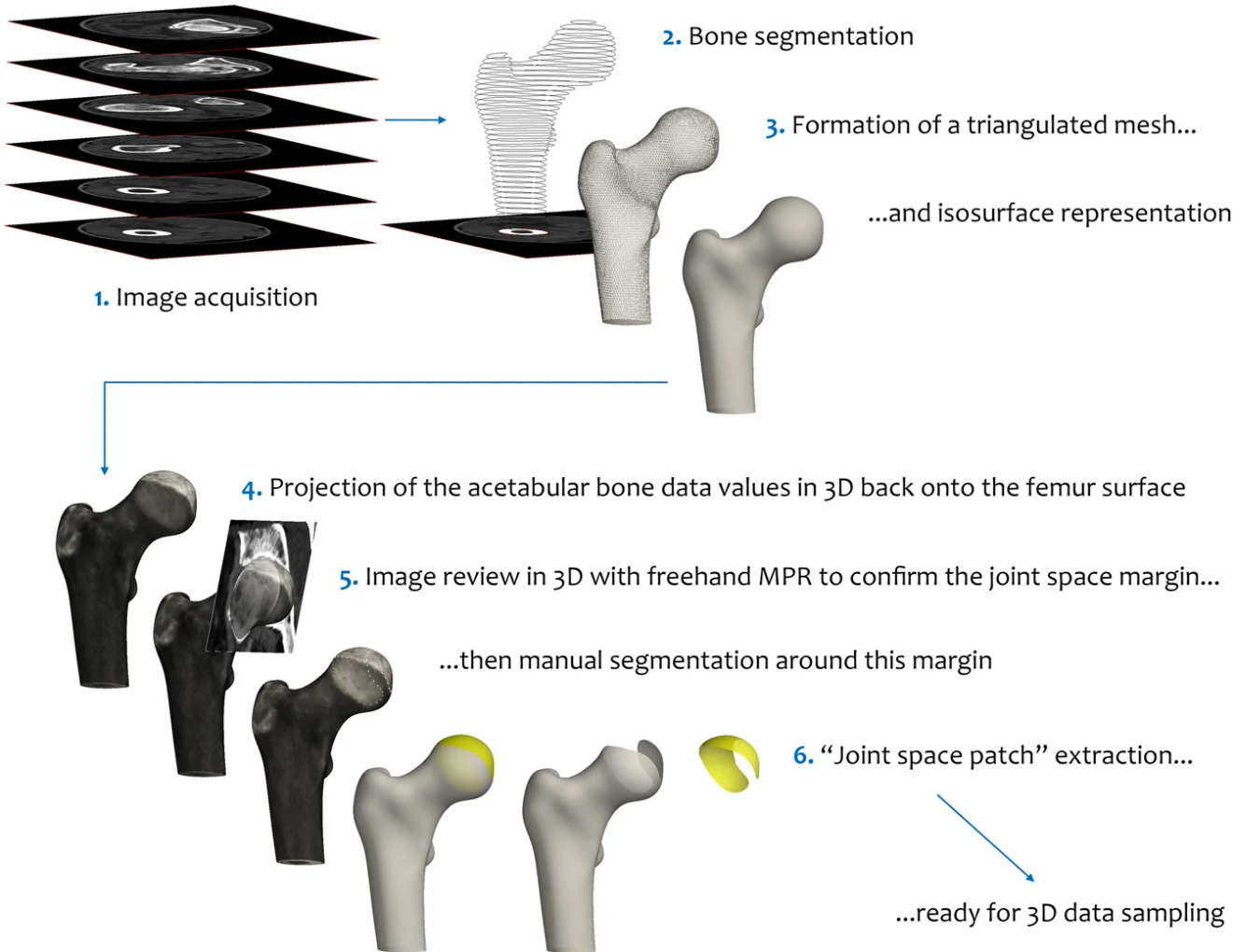


Figure 2: Extraction of the joint space patch (Turmezei et al. 2018).

ensure that the perimeter of the joint space matches with the cut-out joint space patch, improving reproducibility of the technique. This is illustrated in Figure 2 (step 5) and Figure 3.

1.3.2 3D Joint Space Data Sampling

As a pre-processing stage, the peak cortical density of the bone is calculated in HU from the CT volume across the joint space patch, according to Treece et al. (2015a). The CT data is then sampled at the vertices of the extracted joint space patch by drawing 1D sample lines normal to each vertex. Each 1D sample results in an interpolated linear density profile. An optimiser then fits a Gaussian function to this interpolated data, assuming the imaging system blur can be modelled as Gaussian in shape. The bone surrounding the joint space is modelled as a double peak (Whitmarsh et al. 2017) in the cortical density. In a deconvolution step (Treece et al. 2010; Treece et al. 2012), the optimiser removes the blur to obtain a model of the cortex described as a combination of two step

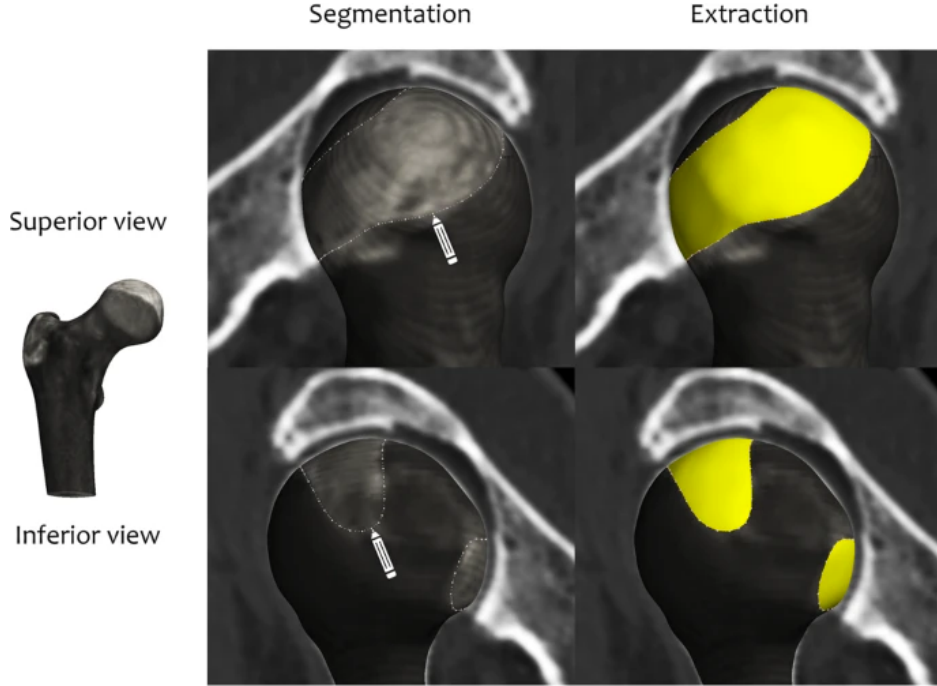


Figure 3: Extraction of joint space patch and perimeter verification (Turmezei et al. 2020).

functions. These step functions have the same peak value due to the fixed peak cortical density constraint imposed at the pre-processing stage. The joint space width is then delivered as the distance between the outer subchondral bone layers, represented by the edges of the step functions, as depicted in Figure 4.

Smoothing of the JSW values at vertices is required to reduce noise and interpolate data over vertices where the optimiser failed to converge to a Gaussian fit. These values can then be viewed as a colour map on the joint space patch and be used to create outer and inner joint surfaces, representing the opposing bones in the joint space, namely the proximal femur and acetabulum.

1.3.3 Success of Joint Space Mapping

Turmezei et al. (2018) evaluated the performance of JSM against the current benchmark of high-resolution peripheral quantitative CT (HRpQCT) for extracting joint space width values from clinical CT of cadaveric hip specimens. The following successful outcomes of JSM were quantified:

1. The joint space width values output by JSM systematically overestimated those output by the gold standard method by +0.13 mm. This was because of a few outlier hips with lower JSW values and very low estimated cortical density at the joint space. Despite this, the accuracy was still below the in-plane pixel spacing of 0.31 mm, and the out-of-plane slice thickness of 1.5 mm.

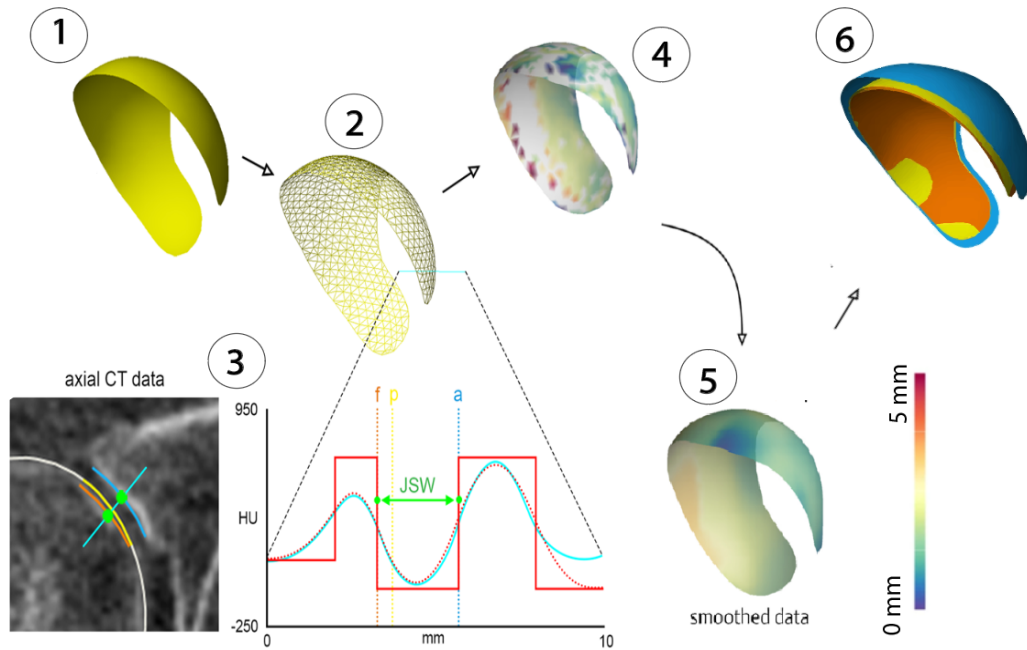


Figure 4: 3D Joint space data sampling (Adapted from Turmezei et al. (2018) and Turmezei et al. (2020)).

1: The joint space patch **p** from Figure 2.

2: JSM algorithm is run on the patch object (**p**). CT data is sampled perpendicular to each vertex of the joint space patch mesh.

3: Each 1D sample line results in an interpolated linear density profile —. The optimised blurred model is shown as - - - and the deconvolved fit leads to the step functions —. JSW is delivered as the distance between the edges of the two step functions, corresponding to the femoral head surface (**f**) and acetabular surface (**a**).

4: Raw JSW values are mapped onto the acetabular surface.

5: JSW values are smoothed to obtain the final colour map.

6: Femoral (**f**) and acetabular (**a**) joint surfaces are created from smoothed JSW values, with the distance between them equal to the JSW.

2. For a multistage process, JSM delivers very precise measurements of joint space width in 3D. The method demonstrated an overall precision of ± 0.32 mm, with the best performance achieved in the inner joint space regions, with precision values around 0.2 mm.

To test the reproducibility of manual stages of JSM, the performance of two operators was compared in carrying out JSM on 30 hip joints, keeping segmentation of the proximal femurs as a non-varying factor. The method demonstrated an inter-operator reproducibility bias (mean of the

difference between the two operators' measurements) of near zero, with the smallest detectable difference of less than 0.2 mm at the inner joint space regions, which is the main region of interest for OA characterisation. These values are superior to the reported best of 0.45 mm for 2D radiographic joint space width assessment at the hip (Ornetti et al. 2009). This is in part because the process allows the femur segmentation to have a precision error of about 2 mm from the actual cortex (Treece et al. 2015b), ensuring a robust tolerance for reproducibility of the technique.

In their study of the applications of JSM in predicting future OA in patients, Turmezei et al. (2020) have shown that the 3D joint space profile is significantly affected by future total hip replacement (THR), with the JSW being significantly lower across the superior joint space in individuals who later underwent THR. The superior performance of JSM to current diagnostic and predictive techniques was demonstrated as the following benefits in joint and disease characterisation:

1. As a 3D measure of joint space width, JSM shows superior predictive capabilities than 2D techniques for THR. It also reveals the 3D displacement of the hip joint as it fails. It was found that the femoral head migrates anterosuperiorly as the OA progresses, widening the posterior joint space. Researchers have struggled to form a similar link between structural disease and clinical status using the limited capabilities of 2D techniques.
2. Complementing JSM with statistical shape modelling (SSM) revealed significant differences in the shapes of acetabula that belonged to THR cases, which were significantly broader across the anterior and posterior regions of the joint space.
3. A predictive model for future THR developed using combined 3D parameters of relative minimum 3D JSW and cohort acetabular shape data, extracted from statistical shape modelling, outperformed models using radiographic gold standards of KL grade and relative minimum 2D JSW by about 12% in the area under the ROC curve. The predictive capabilities of this model were even stronger with the incorporation of KL grade along with the 3D JSM parameters.

The studies discussed above have shown that JSM has increased reliability compared to current radiographic practices and presented evidence of the potential that encompassing 3D information in OA assessment can hold. More broadly, the technique can serve as a useful tool for screening populations predisposed to joint disease progression due to pre-existing arthritis, shape disorders or professions leading to high stress-loading in the joints. Since JSM is still a relatively novel technique, there is much scope to explore its utility in disease stratification, therapeutic monitoring and prediction of disease in other joints. Along with utility, the method also needs to demonstrate robustness to inconsistent joint positioning and changes in load-bearing (supine vs standing), which

has not been investigated in prior studies.

1.3.4 Knowledge Gaps in the Study of JSM

In all of the previous studies concerned with the validation, applications and feasibility of joint space mapping, there was no prior standardisation of the hip joint positioning for CT acquisition, and any prospectively collected data was just assumed to be polluted with noise generated through uncontrolled positioning.

A radiographic study (Goker et al. 2005) showed that small variations in the hip joint position might not significantly affect the joint space width. While changing from neutral positioning to 15° of flexion had no statistically significant effect on the joint space, a 30° flexion of the hip significantly increased the joint space width by about 0.15 mm. Tom et al. (2016) have shown that in metacarpophalangeal joint positioning, the root mean square of variance is less than 5% for an angle difference of less than 20°. This means that joint positioning has little effect on the average joint space width.

During CT acquisition, it is difficult to perfectly neutralise the patient's position, which can be impacted by several confounding variables. For example, deformities in the hip joint or injuries causing articular pain or swelling may prevent accurate patient positioning. While a straightforward solution for prospective studies is to standardise the patient's position by strapping their feet together, this has the obvious drawback of being impractical for patients experiencing significant pain. Furthermore, it does not yield a satisfactory solution for analysing existing, non-standardised patient scans retrospectively.

It would thus be useful to quantify the tolerance of JSM to the variability in CT acquisition. This would increase confidence in the results obtained via retrospective analysis of joint space maps wherein the patient positioning was within the tolerance limit of the technique. It seems fitting that a similar study to the ones mentioned above be carried out for JSM since this would further enhance the scientific community's confidence in the measurements obtained through JSM, its technical validation, and its applications. The 3D nature of this technique promises to reveal interesting insights into the relationship between joint positioning and the 3D joint space.

This project carries out a sensitivity analysis of JSM with respect to hip joint rotation and aims to quantify the dependence of the technique on consistent joint positioning. Figure 5 illustrates the main aim of this project: to determine whether the joint space width profile for a patient with repeat scans changes with hip rotation.

In the following investigations, we have quantified hip rotation with a suitable metric (a rotation

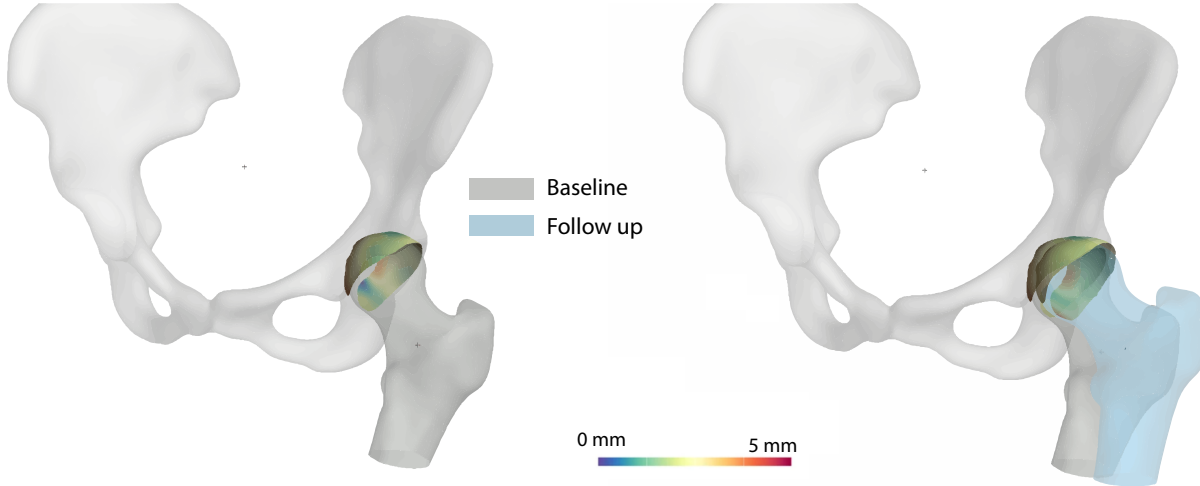


Figure 5: A hip joint with repeated CT scans.

(Left) The joint space width mapped on the femoral head from the baseline scan. The colour bar indicates the magnitude of the distance between the opposing femoral and acetabular surfaces.

(Right) The patient's hip has rotated between the baseline and follow-up scans, and the JSW profiles for each scan are mapped on the femoral head.

matrix), extracted the joint space profiles for each patient in a longitudinal study, and determined whether inconsistent joint positioning significantly affects the hip joint space maps. It is worth noting that the investigations carried out in this project are specific to the hip joint and may not generalise to other joints, which may need to be investigated independently.

2 Theory and Design of Experiment

2.1 Patient Demographics

For this project, we have used CT data available from a longitudinal study of a cohort of 101 individuals, with an average of 36 days between the baseline and follow-up scans. The 60 male and 41 female individuals had a mean age of 65.9 ± 13.6 and varying degrees of osteoarthritis in their hips.

The limited timescale of the project meant no stratification could be carried out based on age or sex. However, it was necessary to exclude particular hips from the study according to the following exclusion criteria:

1. Movement artefacts (4 hips).
2. KL grade (Kellgren et al. 1957) of 4 (14 hips). These hips represent severe disease, with

JSW reducing to zero in some regions of the joint space. While JSM has proven to be very precise even at advanced stages of the disease, it was decided to exclude these hips because the method can sometimes fail in regions of zero JSW.

After exclusion according to the above criteria, we had 386 hip joints that were used in the investigations carried out for this project.

2.2 CT Data

X-ray computed tomography (CT) allows direct visualisation of slices through a 3D attenuation field. This is demonstrated in Figure 6. Each pixel in a slice represents the CT number of the body at that point in space. The following expression is used to find the CT number in HU:

$$\text{CT number in HU} = \frac{\mu - \mu_{H_2O}}{\mu_{H_2O}} \times 1000 .$$

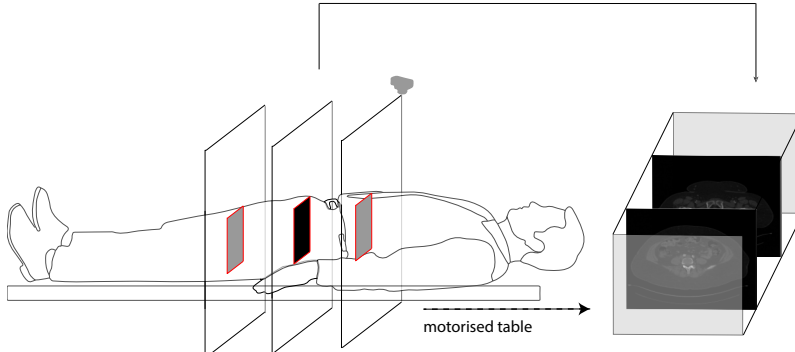


Figure 6: CT data acquisition and representation. The image data is acquired one slice at a time. The resulting dataset is composed of several slices, with a predefined separation between each slice. Since the data is anisotropic, with a higher resolution within each slice than perpendicular to it, interpolation techniques are necessary to retrieve pixel values *between* slices to generate reslices out-of-plane from the original slices.³

Here, μ represents the linear attenuation coefficient of the medium being scanned. CT numbers range from -1000 HU for air to 0 HU for water and 1000 HU for bone. Each pixel in a slice is displayed as a grey level between 0 and 255. Thus, the CT number needs to be quantised such that -1000 HU is mapped to a black pixel and 1000 HU to white.

All CT scans were acquired helically in a supine position using a variety of CT scanners, most of

³ Adapted <https://stock.adobe.com/uk/search?k=person%20lying%20down>

which were Siemens models with Flash capability⁴, with the following parameters: 120 kVp, 1 mm slice thickness, pitch of 0.8, pixel size of 0.924 mm and reconstruction matrix size of 512×512 . These acquisition parameters are not exactly consistent with those used in Turmezei et al. (2018) and Turmezei et al. (2020). However, JSM is robust to these slight variations (Turmezei et al. 2018). Importantly, patient hip positioning was not standardised at the time of acquisition.

2.3 Mesh Representation of the Hip Joint

A triangulated mesh is a collection of vertices, edges and triangular faces representing the surface of a 3D object. Conventional representation renders the mesh faces; however, if edges are rendered instead of the faces, the model becomes a wireframe model. Each vertex, edge and face can be identified by a unique index.

A 3D model of the hip joint was needed for the calculation of hip rotation. The triangulated meshes of the femur and pelvis were used for this purpose. A rotation matrix between their coordinate systems was calculated and used to measure the hip joint rotation.

Figure 7 shows the triangulated mesh representation of the proximal femur and pelvis. In the subsequent investigations, the sacrum of the pelvis (shown in yellow in Figure 7) had no relevance, as will be demonstrated by the coordinate system definitions, and will therefore be left out in illustrations and discussions regarding the pelvis.

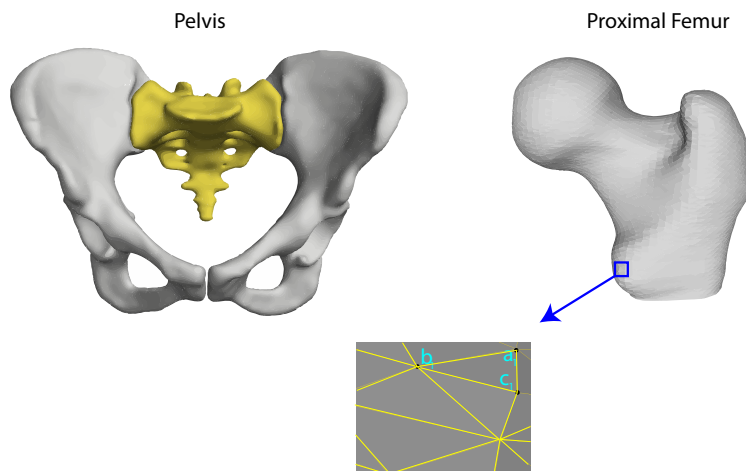


Figure 7: A triangulated mesh representation of the pelvis and proximal femur. Triangles represent the surface of a 3D volume in a triangulated mesh representation. Each vertex, edge and face can be uniquely identified by an index.

⁴<https://www.corporate.siemens-healthineers.com/>

2.4 Method Overview

The steps taken to determine the effect that consistent hip positioning has on the output of JSM are outlined in Figure 8. Each of these steps is explained in detail in Sections 3-6. Four software tools were used to complete the bulk of the project work:

1. *Stradview* is a free-to-use software developed by the Medical Imaging Group of the Machine Intelligence Laboratory at the University of Cambridge. It was used for CT data manipulation to acquire a triangulated mesh representation of the pelvis and femur bones. The majority of the technical work for calculating the hip joint rotation involved implementing new code to *Stradview*'s codebase, written in C++. This is detailed in Sections 3.2 and 5.
2. *wxRegSurf*⁵ is a program that can register pairs of bone meshes by transforming one of them to match the shape of the other as closely as possible. This was useful in creating a statistical shape model for the pelvis, as well as transferring the JSM data from each patient's acetabular surface onto a canonical acetabular surface so that a statistical analysis could be carried out. Statistical shape modelling and the spatial normalisation of JSM measurements are detailed in Sections 3.4 and 6 respectively.
3. *Blender*⁶ is an open-source program that facilitates the 3D graphical rendering pipeline. *Blender* has an embedded python interpreter, which allows python scripts to extend its functionality. The versatility of this software facilitated devising a coordinate system definition for the femur meshes, as detailed in Section 4.3.
4. *MeshLab*⁷ is an open-source program for processing and manipulating 3D triangulated meshes. It was used for mesh simplification, a process that is useful for statistical shape modelling, as detailed in Section 3.3.
5. MATLAB was used to carry out statistical parametric mapping using the *Surfstat* package (Worsley et al. 2009), to determine the effect of hip rotation on the 3D JSW. The details of this approach are explained in Section 6.

⁵<https://mi.eng.cam.ac.uk/~ahg/wxRegSurf/>

⁶<https://www.blender.org/>

⁷<https://www.meshlab.net/>

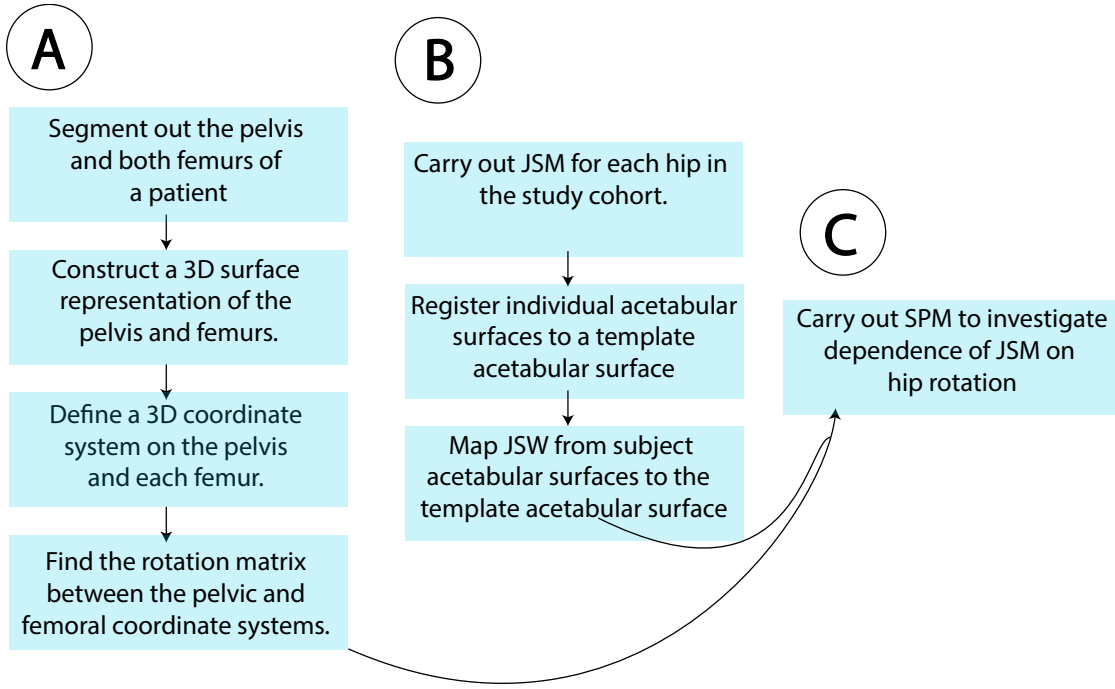


Figure 8: Overview of the investigation of the effect of hip joint rotation on JSM.

- A. Steps involved in quantifying the hip joint rotation.
- B. Finding the 3D JSW for all hips and spatial normalisation.
- C. Statistical analyses.

3 Statistical Shape Modelling

The prevalent manual approach for finding femur rotation at the hip is using 3D reconstruction image viewing software. The clinical hip angle measurements are then made against user-defined orthogonal planes that form an intrinsic image space coordinate system comprising of the axial, coronal and sagittal planes. Having the ability to build 3D meshes from the CT data, we devised a semi-automated method to quantify hip joint rotation that was less prone to operator bias and based on pre-defined coordinate systems for the pelvis and femur.

3.1 Motivation - 3D Surface Extraction

In order to extract the femoral and pelvic surfaces from the 3D data, the following three steps need to be carried out in *Stradview*:

1. In the CT slices, segment out the relevant bone from the background. This can either be done by manually outlining the object of interest or by using an intensity threshold. Bones are represented by higher grey level values in CT representation and can be segmented by thresholding above a certain pixel intensity level and automatically drawing contours around the

thresholded regions. Such surfaces with a certain intensity threshold are called iso-surfaces.

2. Since CT data is anisotropic, we need to interpolate between the data slices to generate a set of contours that represents the surface better than the original sparse contour set. This step will create an interpolation grid according to a user-defined resolution. This resolution affects the speed of the computation, the number of triangles and thus the amount of detail in the extracted surface. This step can be carried out automatically in *Stradview*.
3. Triangulate a surface through the set of contours using a regularised marching tetrahedra algorithm (Treece et al. 1998).

Steps 2 and 3 are automated in *Stradview*. Step 1 is the most time intensive because there is noise in the CT data, and even automatic contouring via intensity thresholding needs manual editing to clean up the contours. As mentioned in Section 2.1, this longitudinal study involved a total of 386 hips (baseline and follow-up), requiring segmentation of 193 pelvises and 386 proximal femurs. This is potentially cumbersome and motivates an approach to speed up this process by fitting a Statistical Shape Model (SSM) of each bone to the CT data. This model could be rotated, scaled and warped to fit the CT data precisely. Contours from this model could then be mapped back on the CT data, thus segmenting out the object of interest.

3.2 Segmentation of the Pelvis in *Stradview*

The first step in extracting the hip joint iso-surface as a triangulated mesh was to segment the pelvis from CT data using *Stradview*. Since there were 193 pelvises for which this process was to be repeated, three approaches were implemented to speed it up:

1. A unilateral segmentation was carried out, i.e. only the left *hemipelvis* was segmented, as seen in Figure 9. Literature suggests most patients have symmetrical hips (Goker et al. 2005) and a simple reflection of the unilateral hemipelvis mesh did, in fact, yield a good fit on the opposite side. The extreme patient cases were dealt with manually with some deformation applied to the reflected unilateral hemipelvis.
2. *Stradview*'s model fitting functionality, wherein a 3D mesh can be fitted to the CT data, was helpful in implementing a bootstrapping approach: the first hemipelvis was segmented out manually to acquire a template mesh that was subsequently used as a hemipelvis model. This model was fitted to new CT data using rotations, scaling and locally affine deformations. This is illustrated in Figure 9.
3. As illustrated in Figure 9's step 1, landmarks are placed in the CT data to align corresponding landmarks on the 3D mesh with the CT data. A new functionality was built into *Stradview*

to allow these landmarks to guide the mesh deformation process (step 4) by putting a weight on the mesh vertices with matching CT landmarks, such that the anatomical landmarks in the CT end up close to those in the deformed mesh. This was found to speed up segmentation rapidly.

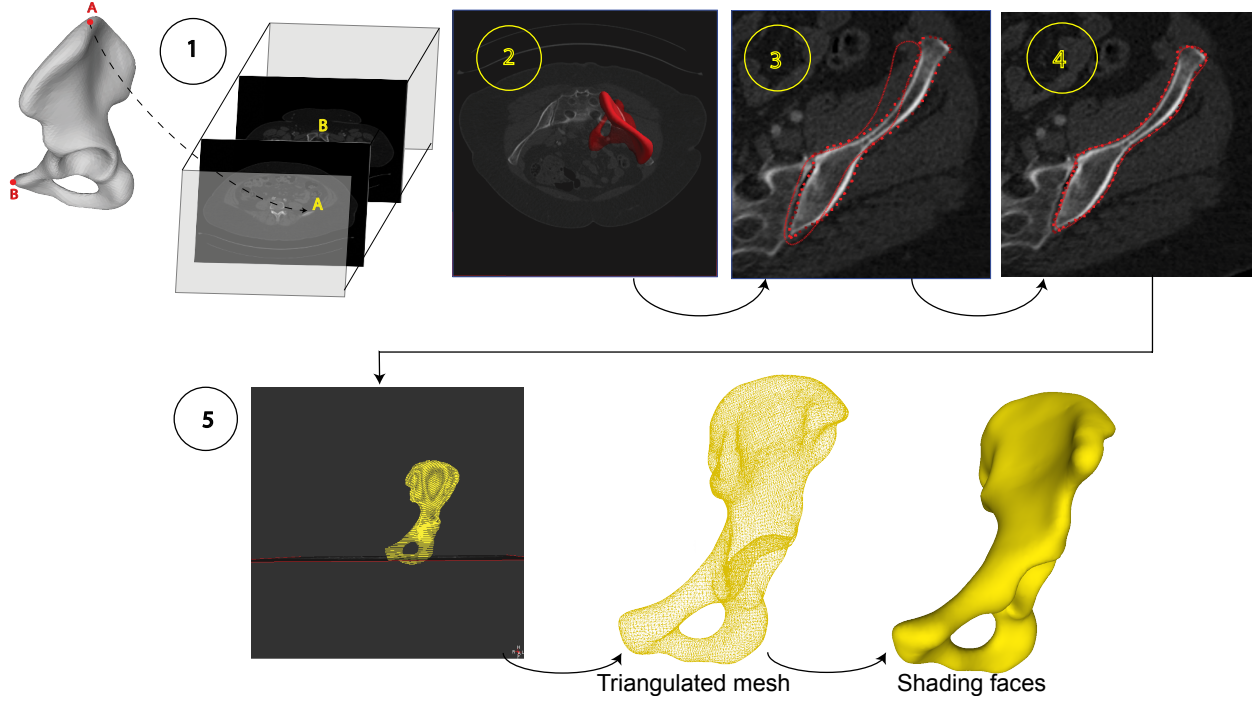


Figure 9: The hemipelvis segmentation process:

- 1) The template mesh has predefined anatomical landmarks. After loading the mesh into *Stradview*, we select corresponding landmarks in the CT data.
- 2) The landmarks in the mesh and CT data are aligned to place the mesh correctly within the CT data.
- 3) There is some misalignment between the CT data and the mesh. The user can semi-automatically outline the hemipelvis in the CT frames (red dots) via thresholding or manual contouring.
- 4) The mesh can be rotated, scaled and warped to fit the red dots outlining the cortical bone.
- 5) The fitted mesh can be mapped back onto the CT data as contours in the CT frames, which can be used to generate a hemipelvis mesh via the regularised marching tetrahedra algorithm.

3.3 Defining a Canonical Hemipelvis

In order to build a statistical shape model, we had to choose the most anatomically average hemipelvis from the set generated by segmentation carried out according to Figure 9 on a sample of the patient data sets. This *canonical* hemipelvis mesh was different from the *template* mesh used in the initial

bootstrapping approach, described in Section 3.2. The template was simply the first hemipelvis that was manually segmented. The surface of the canonical hemipelvis was re-triangulated to a lower resolution (~ 5000 vertices), enough to capture the shape without adding to the computational complexity of surface registration (refer to Section 3.4).

Choosing an average hemipelvis surface by eye is not the only method for obtaining a canonical mesh. We could have also registered this visually average mesh to all the specimens, using *wxRegSurf*, and calculated the mean deformation at each vertex. This mean deformation could be applied to each vertex to yield a mean hemipelvis surface.

Mesh simplification was then carried out in *MeshLab* to identify a set of ~ 700 surface semi-landmarks on the canonical hemipelvis. These were used in the sliding semi-landmark algorithm (Gunz et al. 2005) for registering the canonical mesh to the other hemipelvis surfaces. Mesh decimation ensures the surface semi-landmarks are a suitable subset of the vertices of the original mesh. Figure 10 illustrates the process of mesh simplification.

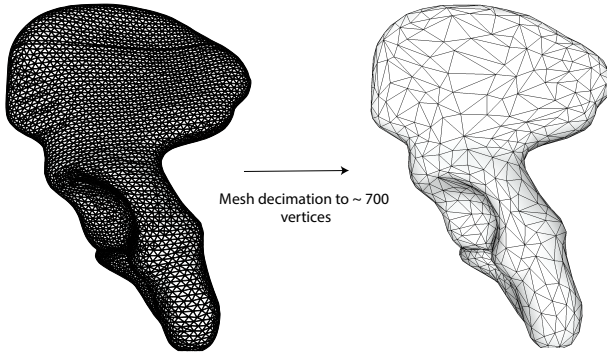


Figure 10: Edge collapse decimation removes some of the edges in the mesh turn by turn until the desired number of triangles is achieved. The vertices of the simplified hemipelvis mesh are extracted as surface semi-landmarks. The simplification process preserves the surface geometry of the hemipelvis maximally.

3.4 Building a Statistical Shape Model Using *wxRegSurf*

A statistical shape model was created after extracting enough hemipelvis surfaces to capture a significant amount of shape variation between patients. This is illustrated in Figure 11. This shape model then underwent a subsequent retraining process: as more hemipelvis surfaces were extracted, the training set grew, and the shape model was updated.

In order to develop an SSM, the canonical hemipelvis was registered in turn to all the meshes in the training set. Surface registration was carried out using a similarity (non-deformable) transformation with an iterative closest point (ICP) registration algorithm, followed by the sliding semi-landmark

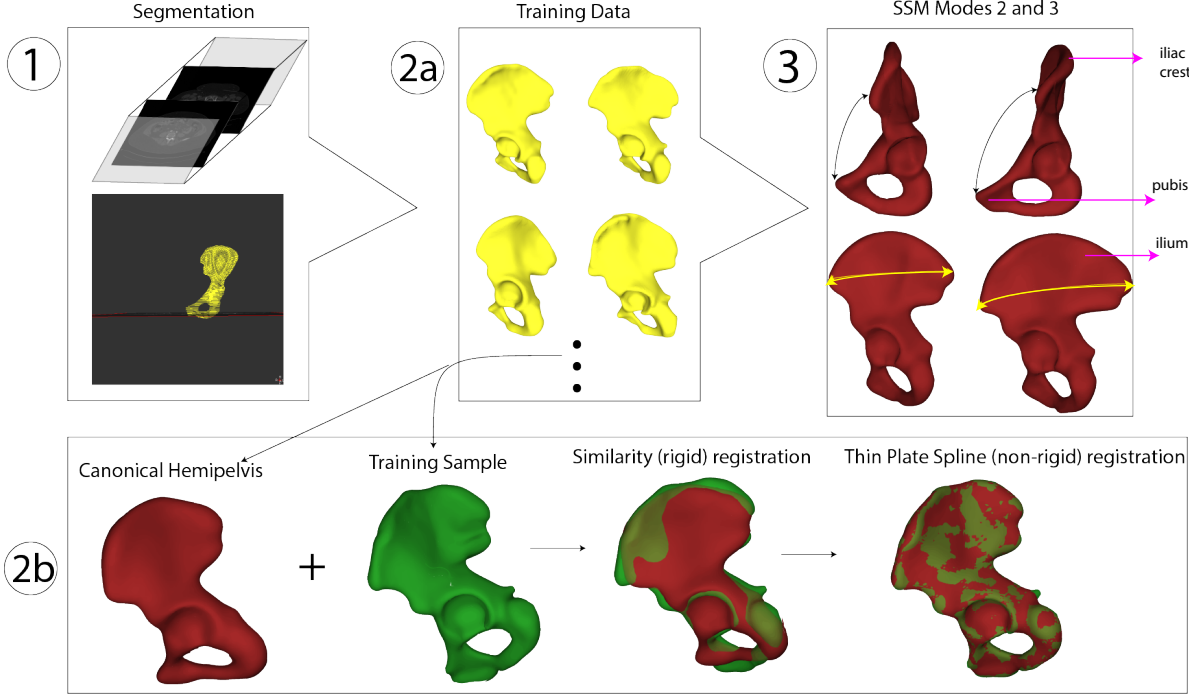


Figure 11: Statistical hemipelvis shape model generation.

(1 & 2a) Segmentation and surface mesh representation to generate training data.

(2b) Canonical mesh registered in turn to all the training samples using the sliding semi-landmark algorithm.

(3) Two statistical shape modes of variation shown, one mode per row. Mode 1 (not shown here) represents size variation.

algorithm. This algorithm minimises the bending energy of the thin plate spline that warps the canonical surface semi-landmarks onto each specimen (Gunz et al. 2013). These steps were performed in *wxRegSurf*.

Since we are working with triangulated meshes, registering the canonical hemipelvis to each of the training set meshes yields a 3D vector for each vertex on the canonical mesh as it is displaced towards the other mesh. The deformed vertices are aligned with the non-deformed canonical vertices by a Procrustes analysis (Goodall 1991) and rescaled by their centroid size so that any variation in size can be captured in the model. Principal component analysis (PCA) is then performed on the vertex sets to extract the mean hemipelvis shape model and orthogonal modes of shape variation. These steps can be automatically performed in *wxRegSurf* to yield an SSM with $n - 1$ principal modes of shape variation, where n is the training set size.

The SSM built using a subset of all the patients' hemipelves sped up the segmentation of further

pelvises (a hemipelvis and its reflection made up a pelvis). In step 4 of Figure 9, the mesh could now be deformed using statistical shape model (SSM) registration, which uses pre-defined transformations to constrain the mesh deformation to common anatomical differences in hips. Common statistical shape modes could characterise the elongation of the iliac crest in the hemipelvis mesh or the variation in the rotation between the ilium and pubis since these are common anatomical differences between the patient’s hips, as depicted in Figure 11. During model fitting, the canonical mesh \mathbf{H} is expressed as a linear combination of the shape modes \mathbf{m}_i , $i = 1, \dots, n - 1$:

$$\mathbf{H} = \mathbf{H}_0 + \sum_{i=1}^{n-1} D_i \mathbf{m}_i$$

where \mathbf{H}_0 is the mean hemipelvis shape model and D_i are the deformation parameters.

3.5 3D Surface Representation of the Femur

We also needed the proximal femur meshes for all patients to define the femoral coordinate system. However, these were less time consuming to acquire (~ 5 minutes per femur) since we already had a well-developed proximal femur SSM trained on a large dataset. The shape model was created in a similar way to that of the pelvis. Figure 12 shows how the shape model was used in this project to retrieve a 3D surface representation of each individual’s femur.

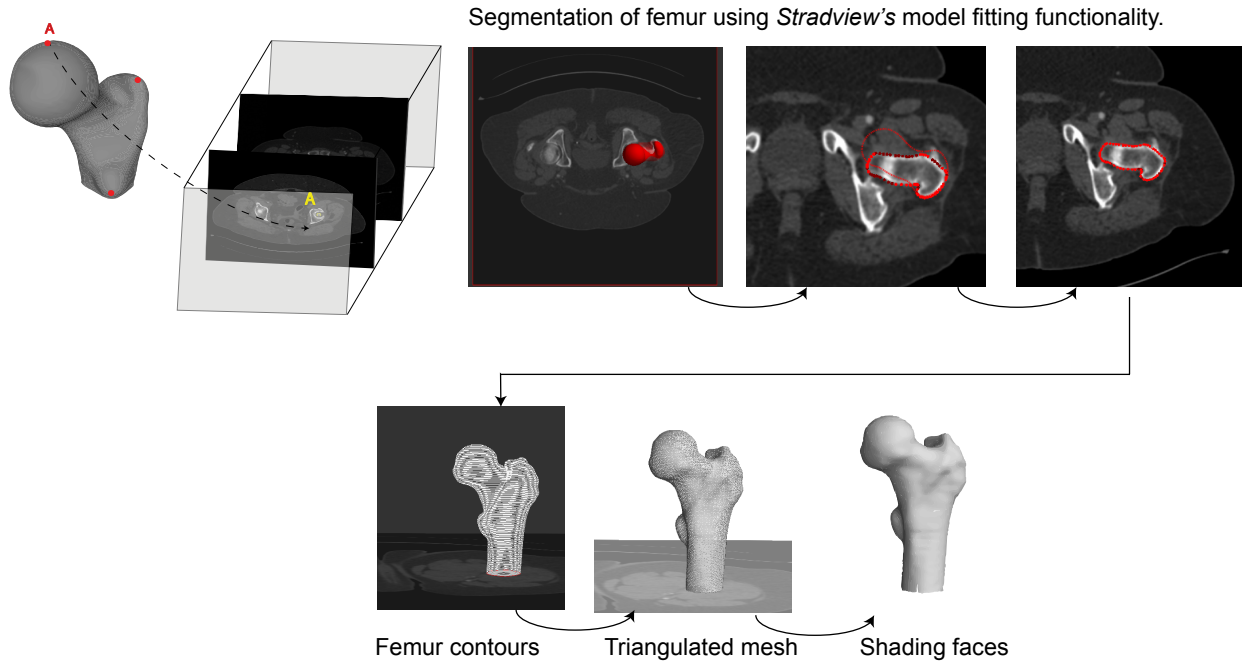


Figure 12: Extracting a 3D surface representation of femurs in the study cohort.

4 Coordinate System Definitions

4.1 Use of Anatomical Landmarks

Anatomical landmarks are biologically meaningful points in the human body and determine homologous parts of the body, thus preserving correspondence between different specimens. Most of these landmarks are relatively easy to identify in a CT scan. To find hip joint rotation, we explicitly defined and standardised the anatomical coordinate reference frames for the pelvis and femur. The position and orientation of these anatomical frames were determined using visible anatomical landmarks on the bones. Landmarks that were easiest to identify in CT data were used for coordinate system definitions to ensure repeatability in locating them between trials. Common anatomical landmarks in the proximal femur and pelvis are shown in Figure 13. Some of these were used in the coordinate system definitions which are described in Sections 4.2 and 4.3.

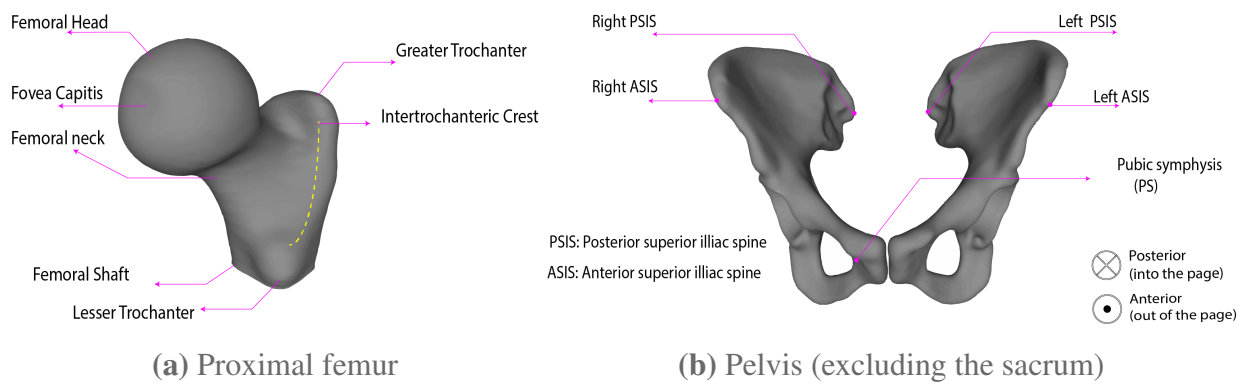


Figure 13: The anatomy of the human pelvis and proximal femur.

4.2 Pelvis Coordinate System

Once we had a 3D mesh for the pelvis, we defined a coordinate system according to Figure 14. This coordinate system is widely used (Cappozzo et al. 1995) by radiologists for manual measurement of the hip joint rotation. We used the same definition to ensure consistency, despite having incorporated a different, semi-automated hip rotation measurement technique.

First, the origin is defined as the midpoint of the pubic symphysis (PS). The x -axis is defined as the line joining the origin to the midpoint of the line joining the left and right anterior superior iliac spines (ASIS). The y -axis is defined as lying in the sagittal plane and perpendicular to the x -axis. The sagittal plane is defined as the plane containing the following three points: the midpoint of the PS, the midpoint of the ASIS and the midpoint of the posterior superior iliac spines (PSIS). These points are illustrated in Figure 14. The z -axis is then retrieved by orthogonality.

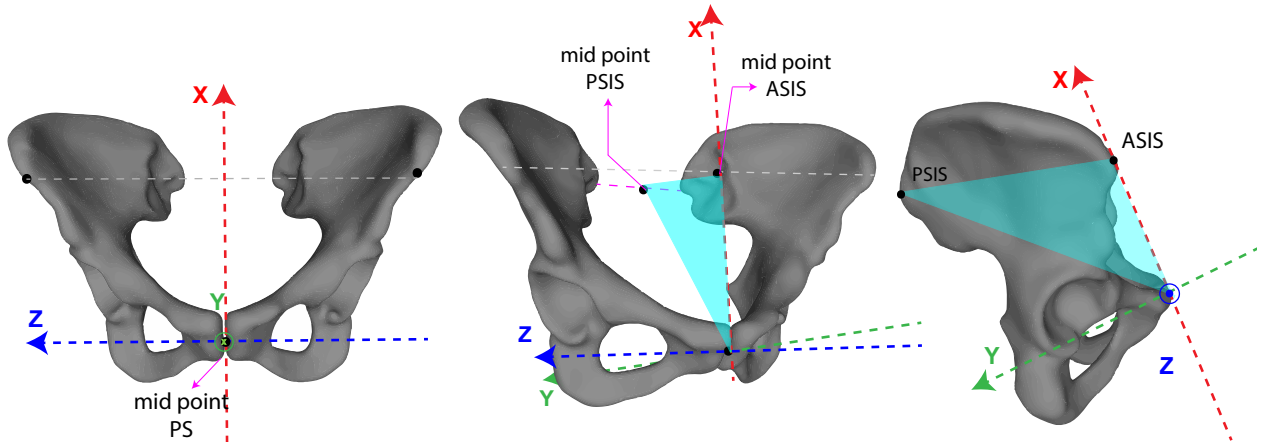


Figure 14: Definition of the pelvic coordinate system.

4.3 Femur Coordinate System

4.3.1 Femoral Neck Axis

Initially, the femoral coordinate system was simplified to finding the neck axis. A standard technique for femoral neck axis definition, outlined in (Davda et al. 2011), was used. The femoral neck axis can be extracted from the proximal femur mesh in the following steps:

1. Firstly, the centre of the joint's rotation was found by fitting a best fit sphere to the femoral head in *Blender*. As shown in Figure 15 (1 & 2), the average of ~ 60 vertices of the femur mesh was used to define the centre of the femoral head. These vertices were picked as those with the lowest registration error and forming two planar rings around the best fit sphere.
2. Figure 15 (3) shows how the femoral neck axis was defined. The intersection between the sphere and femoral neck defines the head-neck junction, and a ring of vertices demarcating this junction was chosen. Another ring of vertices was selected at the base of the neck, along the edge of the inter-trochanteric crest. A weighted average of these rings was used to find the centre of the femoral neck. Different definitions of the femoral neck axis exist in literature (Zhang et al. 2020; Hartel et al. 2016), and using a weighted average approach gave us the flexibility to adapt the neck axis according to each definition. The exact weighting used in the final investigations was decided in liaison with a radiology expert.
3. Finally, the neck axis was defined as the line joining the centre of the femoral head to that of the neck.

The femoral head centre was deliberately found as the average of the vertices of the femoral head, not the sphere. This allowed for a method to accelerate finding the neck axis for each femur in the

study cohort.

Repeating the process illustrated in Figure 15 for 386 femurs is time-consuming. Therefore, the IDs of vertices used to define the neck axis of a canonical femur mesh were found once as described above and saved. This mesh was fitted to each patient’s CT data according to Figure 12, and the femoral neck axis was calculated using the saved vertices each time. A validation study with twenty visibly different femurs was carried out for this approach and is discussed in Section 7.1.

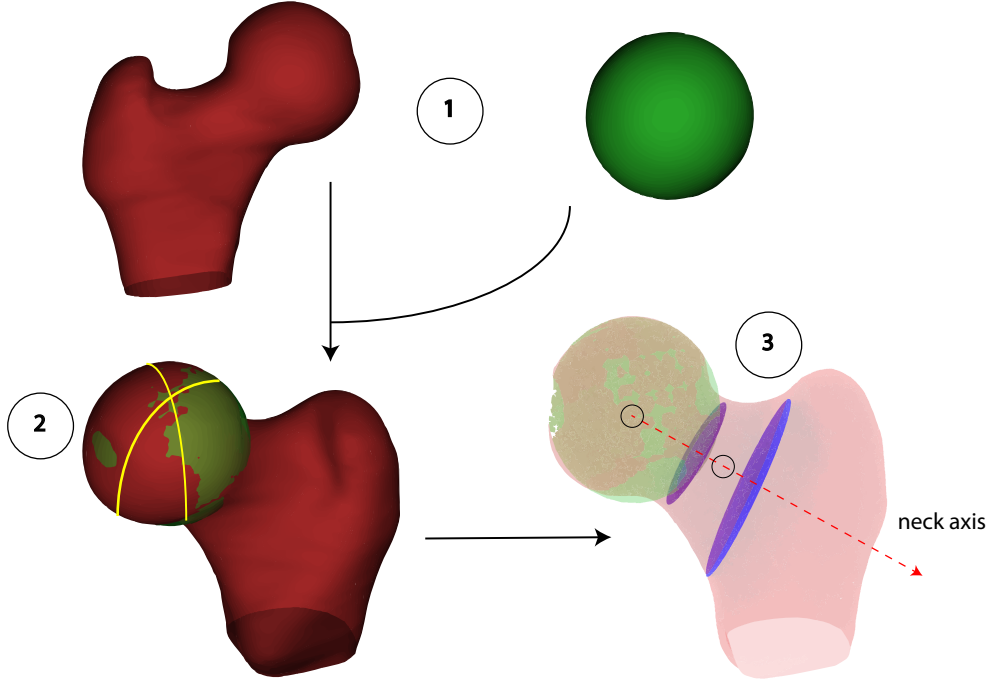


Figure 15: Definition of the femoral neck axis

4.3.2 3D Femoral Coordinate System

The femoral neck axis, a 1D vector, is not sufficient to measure hip rotation in three independent directions. Clinical practice involves projecting this neck axis onto three pre-defined orthogonal planes, set with respect to the pelvis (refer to Section 5.1), to extract the magnitude of abduction/adduction, internal/external rotation and flexion/extension of the hip. However, these three angles are not independent since knowing any two angles (and the neck axis) is sufficient to evaluate the third. Incorporating these angles in statistical tests that ignore their correlation can lead to biased estimates of the test statistic. This bias can cause invalid inferences to be made regarding the effects of hip rotation on JSM.

Therefore, a 3D coordinate system for the proximal femur was defined to circumvent this problem, such that elementary linear algebra could yield a set of three independent angles corresponding to

hip rotation. The international standard femoral coordinate system (Wu et al. 2002) recommended by the International Society of Biomechanics, while widely used, is defined with respect to the entire femur. We needed a coordinate system for the upper third of the femur that could be easily defined using the neck axis definition established in Section 4.3.1 and anatomical landmarks clearly visible in CT data. Therefore, a slight adaptation of the approach suggested in Kang et al. (2005) was used. The 3D proximal femoral coordinate system is explained in Figure 16.

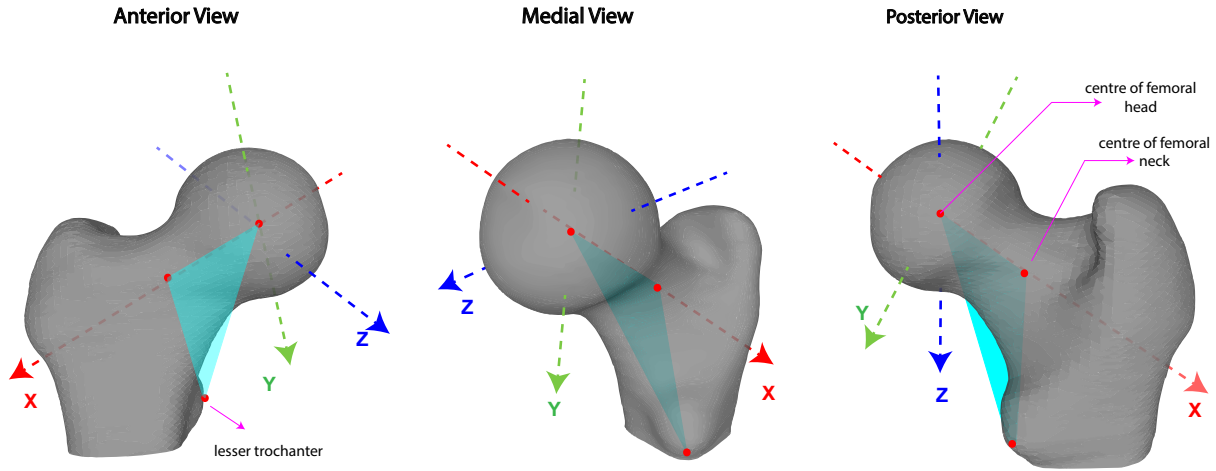


Figure 16: Definition of the femoral coordinate system. The x -axis is defined along the femoral neck axis, which is determined as in Section 4.3.1. The y -axis lies in the plane containing the femoral head and neck centres and the lesser trochanter. The z -axis can be retrieved by orthogonality.

5 Finding the Hip Joint Angle

5.1 Finding Clinically-Relevant Joint Rotation

As mentioned earlier, the clinical practice of finding hip rotation involves defining orthogonal planes formed by the axes of the pelvic coordinate system. The anatomically plausible movements in each plane are listed in Table 1. Each of these movements is illustrated in Figure 1.

One of the benefits of using a 3D surface representation of the hip joint is the ease of analysis and manipulation of the triangulated meshes. By defining the pelvic coordinate system consistently with that used in radiology, this project was able to replicate the clinically-relevant hip rotation measurements using *Stradview*. This semi-automated angulation protocol is shown in Figure 17.

Plane	Positive rotation	Negative rotation
Sagittal (xy)	Flexion	Extension
Axial (yz)	Internal rotation	External rotation
Coronal (xz)	Adduction	Abduction

Table 1: The rotation of the femur in three orthogonal planes.

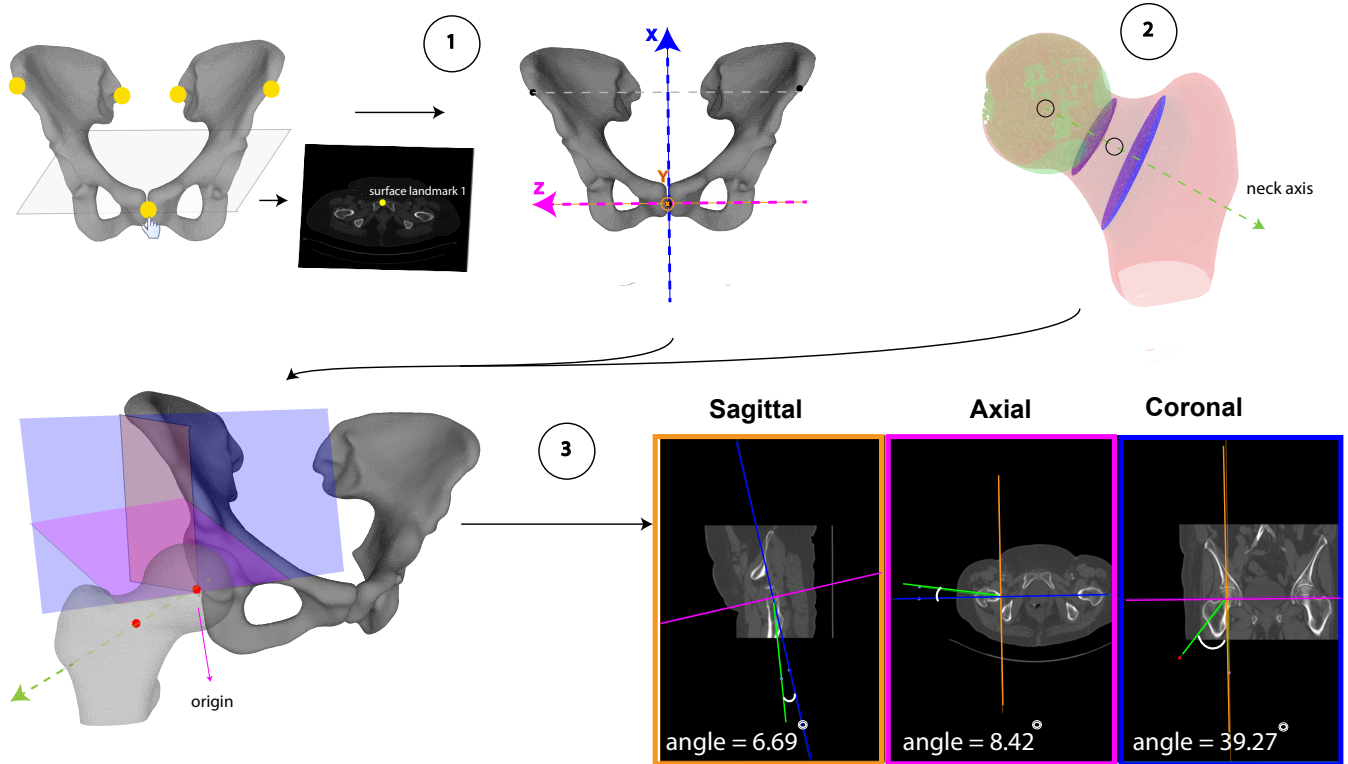


Figure 17: Semi-automatically defining clinically-relevant hip joint rotation.

1. Surface landmarks are placed on the 3D pelvis mesh to define the coordinate axes. Landmark placement can be verified by locating these landmarks in the CT data.
2. The femoral neck axis is defined according to Section 4.3.1.
3. The femoral neck axis is projected into the sagittal, coronal and axial planes in turn and the angle is measured automatically with respect to the axes corresponding to the other two planes.

5.2 Hip Angulation as Composed of Elemental Rotations

Euler angles are a set of three angles used to specify the orientation—or change thereof—of a 3D object. Each of the three angles specifies an elemental rotation around an axis in a 3D Cartesian

coordinate system. In the Tait-Bryan⁸ convention of Euler angles, each angle in the triplet defines a rotation around a *different* Cartesian axis. For example, in the ZYX notation, the first angle specifies rotation around the z -axis, the second around the y -axis, and the third around the x -axis.

As mentioned in Section 4.3.2, the femoral neck axis is not sufficient to measure hip rotation in three independent directions. The three angles acquired clinically by projecting the neck axis onto three orthogonal planes are not independent and represent two rotational degrees of freedom by three values. This approach of characterising hip rotation is very useful clinically, as it allows quantification of anatomically possible hip rotation in three orthogonal orientations. However, incorporating these correlated angles in statistical tests could lead to invalid inferences being made regarding the effects of hip rotation on JSM.

To overcome this problem, we used the 3D coordinate systems for both the proximal femur and pelvis. A rigid body can be transformed from a known standard orientation into any other orientation by composing three elemental rotations. Conversely, a rotation matrix \mathbf{R} , parametrised by three Euler angles, can be used to represent this mapping between the two orientations of a rigid body. The latter approach was more suitable for the 3D meshes used in this investigation. The mapping between the pelvic and femoral coordinate systems was delivered as the rotation matrix between the two bones. A quantification of hip rotation was therefore achieved in the following steps:

1. Find the rotation matrix $\mathbf{R}_{world \rightarrow pelvis}$ for transforming a point in \mathbb{R}^3 from the world coordinates into the pelvic coordinate system. This matrix was found by noting that any vector $\mathbf{u}^{(w)}$ can be transformed into $\mathbf{u}^{(p)}$ by using the following relation:

$$\begin{aligned} \begin{bmatrix} u_1^{(p)} \\ u_2^{(p)} \\ u_3^{(p)} \end{bmatrix} &= \begin{bmatrix} \mathbf{e}_1^{(p)} \cdot \mathbf{u}^{(p)} \\ \mathbf{e}_2^{(p)} \cdot \mathbf{u}^{(p)} \\ \mathbf{e}_3^{(p)} \cdot \mathbf{u}^{(p)} \end{bmatrix} = \begin{bmatrix} \mathbf{e}_1^{(p)} \cdot (u_1^{(w)} \mathbf{e}_1^{(w)} + u_2^{(w)} \mathbf{e}_2^{(w)} + u_3^{(w)} \mathbf{e}_3^{(w)}) \\ \mathbf{e}_2^{(p)} \cdot (u_1^{(w)} \mathbf{e}_1^{(w)} + u_2^{(w)} \mathbf{e}_2^{(w)} + u_3^{(w)} \mathbf{e}_3^{(w)}) \\ \mathbf{e}_3^{(p)} \cdot (u_1^{(w)} \mathbf{e}_1^{(w)} + u_2^{(w)} \mathbf{e}_2^{(w)} + u_3^{(w)} \mathbf{e}_3^{(w)}) \end{bmatrix} \\ &= \begin{bmatrix} \mathbf{e}_1^{(p)} \cdot \mathbf{e}_1^{(w)} & \mathbf{e}_1^{(p)} \cdot \mathbf{e}_2^{(w)} & \mathbf{e}_1^{(p)} \cdot \mathbf{e}_3^{(w)} \\ \mathbf{e}_2^{(p)} \cdot \mathbf{e}_1^{(w)} & \mathbf{e}_2^{(p)} \cdot \mathbf{e}_2^{(w)} & \mathbf{e}_2^{(p)} \cdot \mathbf{e}_3^{(w)} \\ \mathbf{e}_3^{(p)} \cdot \mathbf{e}_1^{(w)} & \mathbf{e}_3^{(p)} \cdot \mathbf{e}_2^{(w)} & \mathbf{e}_3^{(p)} \cdot \mathbf{e}_3^{(w)} \end{bmatrix} \begin{bmatrix} u_1^{(w)} \\ u_2^{(w)} \\ u_3^{(w)} \end{bmatrix} \quad (1) \\ \therefore \mathbf{u}^{(p)} &= \mathbf{R}_{world \rightarrow pelvis} \mathbf{u}^{(w)}, \end{aligned}$$

where $\mathbf{e}_i^{(p)}$, $i = 1, 2, 3$ represent the unit vectors in the x, y and z axes directions, respectively,

⁸https://en.wikipedia.org/wiki/Euler_angles

of the pelvic coordinate system. $\mathbf{e}_1^{(w)} = [1, 0, 0]^T$, $\mathbf{e}_2^{(w)} = [0, 1, 0]^T$ and $\mathbf{e}_3^{(w)} = [0, 0, 1]^T$.

2. Find the rotation matrix $\mathbf{R}_{world \rightarrow femur}$ analogously using the coordinate system definition of the proximal femur.
3. Find the rotation matrix $\mathbf{R}_{femur \rightarrow pelvis}$ by noticing that:

$$\begin{aligned}\mathbf{R}_{femur \rightarrow pelvis} &= \mathbf{R}_{world \rightarrow pelvis} \mathbf{R}_{femur \rightarrow world} \\ &= \mathbf{R}_{world \rightarrow pelvis} \mathbf{R}_{world \rightarrow femur}^T.\end{aligned}\tag{2}$$

This rotation matrix can also be found by substituting the basis vectors of each coordinate system into Equation 1.

4. Decompose $\mathbf{R}_{femur \rightarrow pelvis}$ into Tait-Bryan angles in the ZYX notation. *Stradview*'s source code already had an implementation for this, which was reused.

While extracting the Tait-Bryan angles was useful in visualising the joint rotation, the rotation matrix $\mathbf{R}_{femur \rightarrow pelvis}$ was used as the final metric to quantify hip rotation for each patient. This is because it proved more useful in the subsequent statistical analyses. The rotation matrix was used to find the rotation difference between the baseline and follow-up hips in this longitudinal study, as discussed in Section 7.3.

6 Statistical Parametric Mapping (SPM)

Statistical parametric mapping involves conducting spatially-extended statistical tests for hypotheses on regionally specific effects (Friston et al. 1994). It uses a general linear model (GLM) at each point on a surface to explain how a measured quantity varies in terms of an experimental factor. Previous studies have used SPM to characterise the relation between cortical bone parameters and hip fracture type (Poole et al. 2017). This project used SPM to explain the effect of hip rotation on the spatially varying JSW data, mapped onto the joint space patch.

SPM is a voxel-based approach that employs classical inference to characterise regionally specific responses to experimental and confounding factors. Voxel-based analyses assume that the data from a particular voxel all derive from the same region of an object. If such an assumption is violated, biases arise in the voxel values, which may distort the effect of the experimental variable (Friston et al. 1994). Therefore, 3D JSW data from every subject needed to be analysed in a standard anatomical space to enable consistent reporting of region-specific effects.

In order to achieve spatial normalisation, JSW data was mapped onto each subject's acetabular surface and subsequently transferred onto a canonical acetabular surface. This surface was created

using 20 test subjects in the JSM validation study (Turmezei et al. 2018). All acetabular surfaces were registered in turn to this canonical surface, using a rigid similarity transformation followed by a non-rigid thin plate spline deformation (Gunz et al. 2013; Gunz et al. 2005). This was followed by data transfer from each subject’s acetabular surface onto the canonical mesh. This process is illustrated in Figure 18 and was carried out in *wxRegSurf*.

Finally, the JSW data was smoothed after being mapped on the canonical acetabular surface. Smoothing was also carried out before the mapping of data onto the canonical. Smoothing helps reduce noise and cover any missing measurements due to a failed convergence of the JSM algorithm (Turmezei et al. 2020). Furthermore, by the central limit theorem, smoothing ensures errors are normally distributed, thus rendering inferences based on parametric tests more reliable (Friston et al. 1994).

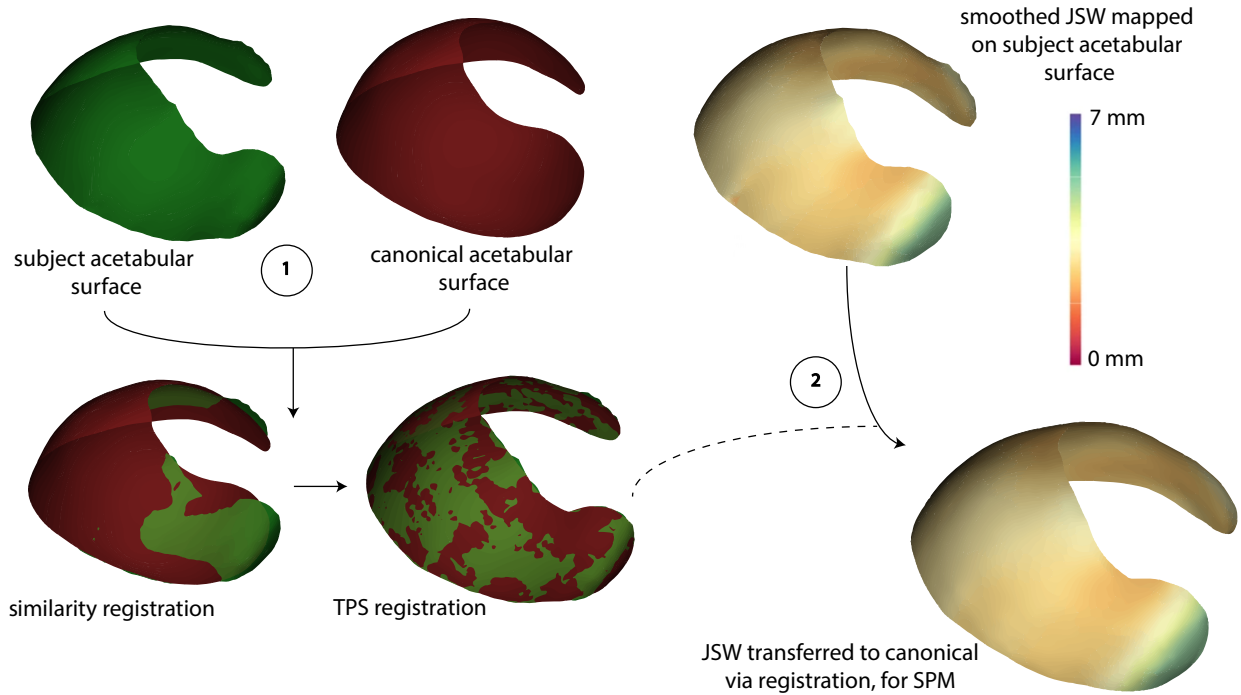


Figure 18: Registration and data transfer to a canonical acetabular surface.

1. The **canonical acetabular surface** is registered to the **subject’s acetabular surface** through a similarity (rigid) and thin plate spline (non-rigid) registration.
2. Smoothed JSW value at each vertex of the specimen is transferred to the nearest vertex of the canonical mesh after registration.

7 Results and Discussion

7.1 Femoral Neck Axis Definition

As mentioned in Section 4.3.1, the femoral neck axis in all 386 hips was found using a pre-defined set of vertices on the canonical proximal femur mesh. These vertices were averaged to find the femoral head and neck centres. The neck axis was subsequently defined as passing through these two points.

To validate the reuse of the same saved vertex IDs for the neck axis definition, a sample of twenty femurs with varying shapes was selected by eye, and the canonical femur mesh was fitted to each femur. The standard approach (Davda et al. 2011), which outputs new vertex IDs to define the neck axis for each femur (as in Figure 15), was compared to the use of a pre-defined vertex set. Since the standard method uses vertices more representative of each individual patient’s anatomy, it is considered more accurate in this investigation.

There was an average absolute offset of $3.13 \pm 2.06^\circ$ between the neck axes acquired using the two approaches for the femurs in the validation study. We chose to accept this small error to ensure automation of finding the femoral neck axis. The process of finding the neck axis of an individual’s femur thus involved only two steps: fitting a canonical proximal femur mesh to the CT data in *Stradview* and finding the femoral neck axis through a pre-defined set of vertices on this mesh.

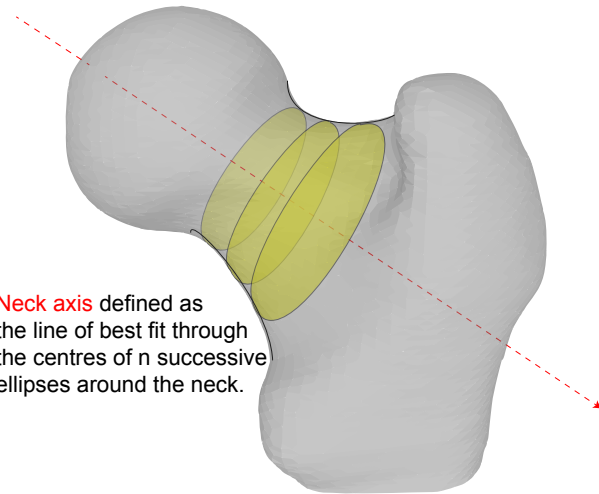


Figure 19: Alternate approach for finding the femoral neck axis.

There are significant differences between 3D mesh-based techniques for finding the femoral neck axis (Zhang et al. 2020). This variation stems from the complex architecture of the proximal femur, resulting from an asymmetric cross-section of the cortical bone between the inferior and supe-

rior regions of the neck (Bonneau et al. 2012). In this project, the definition suggested by the Orthopaedic Research Society (Davda et al. 2011) was used for the femoral neck. This has the advantage of working well with triangulated meshes since it provides an efficient way of acquiring two sets of vertices, one for defining the centre of the femoral head and another for defining the centre of the femoral neck. This femoral neck definition also accounts for the asymmetric neck cross-section.

The technique suggested by Bonneau et al. (2012), illustrated in Figure 19, introduces a model of the femoral neck based on n successive cross-sectional ellipses, which allow the asymmetry in the superior and posterior parts of the neck to be captured more accurately. This method, further validated by Fischer et al. (2020), shows a very high degree of agreement with the 2D approaches of identifying the femoral neck axis, currently used as the default for finding the angle of anteversion and the neck-shaft angle (Mannava et al. 2017). This definition of the femoral neck is analogous to the one used in this project, for $n = 2$.

7.2 Comparison of Manual and Semi-automated Angles

A valuable by-product of defining the 3D femoral coordinate system as in Section 4.3.2, in conjunction with the semi-automated hip rotation protocol, is the technique of finding clinically-relevant rotations by projecting the femoral neck (x) axis onto three pre-defined orthogonal planes. These angles do not form an independent set. Thus, they cannot be used in the statistical analyses of the relation between hip rotation and 3D JSW. However, they are used commonly in clinical practice to characterise joint movement and to standardise patient position for radiographic analyses (Polesello et al. 2011).

For the 386 hips in this study, two clinical observers had also measured the hip joint angles manually using 3D reconstruction image viewing software. These angles quantified the extension/flexion, abduction/adduction and internal/external rotation of each hip. These clinically acquired angles were used to compare the semi-automatic angulation protocol in *Stradview* to a standard approach widely used by radiologists. Even though this set of clinically-relevant angles was not used in the statistical analyses discussed later, it was realised that this comparison would still yield useful insights into the strengths and limitations of the semi-automated approach we devised. These insights could be extrapolated to the rotation matrices found as a measure of hip rotation, using the 3D coordinate system definitions, as discussed earlier in Section 5.2.

The mean and standard deviation for each anatomical rotation, measured for all subjects using the two approaches, is reported in Figure 20. Extension/flexion, measured in the sagittal plane, was underestimated by the semi-automated, with $P = .04$. Similarly, internal/external rotation measured

in the axial plane was higher ($P = .02$), on average, when measured manually compared to using *Stradview*. Finally, our approach yielded a higher average angle of abduction/adduction ($P < .001$) in the coronal plane compared to the manual protocol.

Manual vs Semi-automated Angle Measurements

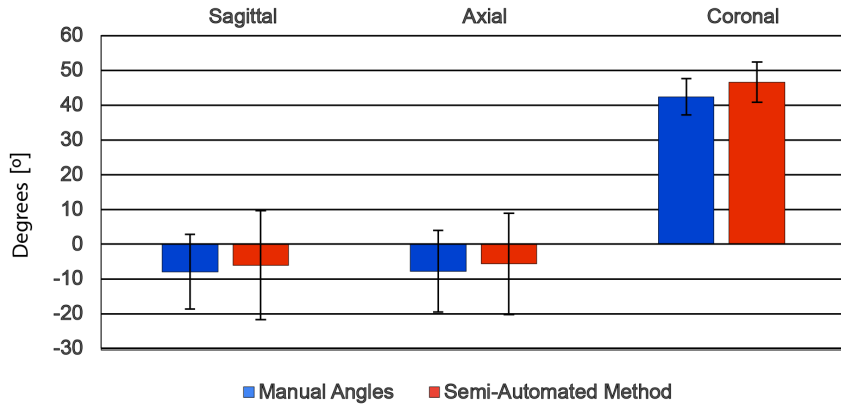


Figure 20: Comparison of the angles acquired manually and semi-automatically in *Stradview*.

A few reasons may contribute to the differences in finding hip rotation manually and using *Stradview*. Firstly, the manual protocol for finding hip rotation involves an ambiguous definition of the femoral neck axis. After defining the sagittal, coronal and axial planes, the observer views CT data by eye and draws a line from the femoral head down the neck, in each plane, at what they know to be the most appropriate location of the neck axis.

Thus, the manual angulation protocol is prone to a significant observer bias, leading to inconsistent angle measurements between operators. The inter-operator bias for this approach was not measurable due to the constraints of the project. However, an intra-operator variability study was carried out to explore the extent of reproducibility bias within this technique. A CT dataset was randomly selected, and the set of three angles was found ten times manually, using a DICOM viewer⁹. The standard deviations in the obtained angles were 9.49° , 11.21° and 5.63° in the sagittal, axial and coronal planes, respectively. In contrast, the semi-automated method produced angles with lower standard deviations of 3.67° , 4.21° and 1.63° in the three planes. This is because the same user is highly likely to place surface landmarks in approximately identical locations between trials for the pelvic coordinate system definition (refer to Figure 17). Furthermore, the definition of the femoral neck axis is highly reproducible due to automation in *Stradview*.

Secondly, the task of defining the femoral neck using a 3D mesh is not trivial. There are many approaches recommended by various studies, as discussed in Section 7.1, and we used one of these

⁹<https://www.osirix-viewer.com/>

many possible definitions. Note that there is no current gold standard for defining the neck axis; clinicians use what they seek as the most appropriate method, while studies involving 3D surface representations of the hip joint usually use a mesh-based method to find the neck axis (Zhang et al. 2020). Further investigations into the accuracy and precision of each approach would be required to make any conclusive remarks.

While there are obvious limitations to the semi-automated method of finding clinically-relevant hip joint rotations, such as varied definitions of the neck axis, the benefits of this technique make it suitable for such measurements. This approach is very efficient and labour-saving: after 3D surface extraction of all hip joints, the hip rotation can be found automatically using a batch file that can be run in *Stradview*. Furthermore, a 3D technique is more suitable to the hip joint phenotype and yields a more representative set of angles than a 2D approach. Finally, this approach allows visualisation of the femoral neck axis using *MeshLab* or *Blender*. A radiology expert could review these visualisations and adapt the algorithm for finding the neck axis to obtain angles more reliably.

For this project, the effect of varied definitions of the coordinate systems was minimised. This is because any consistent measure of hip rotation, which three independent elemental rotations could parametrise, was sufficient for carrying out statistical analyses and avoided incorporating non-independent experimental variables that could bias the test statistic. Thus, the semi-automated technique for characterising hip rotation was deemed very suitable for this investigation.

7.3 Effect of Hip Angulation on JSM Output

SPM was performed on all 386 hips to map out any regions on the 3D joint space that significantly changed with hip rotation. We expected SPM to reveal no significant results when investigating the 3D JSW profile against hip rotation. This is because the inter-patient differences in the spatial distribution of JSW would, on average, cancel out, yielding no observable systematic dependence of the JSW on angulation. Furthermore, longitudinal data requires methods that can adequately account for the intra-subject correlation of the JSW measurements. Therefore, the absolute difference of 3D JSW maps between baseline and follow-up for each hip was used to remove bias from within-subject correlation. This was investigated against the absolute change in hip rotation between the repeat scans.

In order to find the change in hip rotation between the two scans, we leveraged the intrinsic notion of distance on the 3D rotation group¹⁰. This distance is independent of whether the rotation is represented using rotation matrices or unit quaternions. However, it cannot be found by simply subtracting the baseline and follow-up Euler angles since these are highly dependent on the

¹⁰https://en.wikipedia.org/wiki/3D_rotation_group

sequence in which they are applied. Thus, we worked with rotation matrices in our investigation. Let $\mathbf{R}_{p \rightarrow f1}$ and $\mathbf{R}_{p \rightarrow f2}$ represent the rotation matrix of the two femurs in the *same* basis, i.e. with the baseline and follow-up pelvis coordinates aligned. Then the rotation matrix that represents the rotation difference is given by:

$$\mathbf{D} = \mathbf{R}_{p \rightarrow f2} \mathbf{R}_{p \rightarrow f1}^T . \quad (3)$$

We retrieved the angle of rotation between the two femurs by using an axis-angle representation ¹¹: the orientation of the follow-up femur is achieved by rotating the baseline femur through an angle θ about an axis \mathbf{u} where:

$$\text{if } \mathbf{D} = \begin{bmatrix} a & b & c \\ d & e & f \\ g & h & i \end{bmatrix}, \quad \text{then } \mathbf{u} = \begin{bmatrix} h-f \\ c-g \\ d-b \end{bmatrix}. \quad (4)$$

The angle θ is then obtained as $||\mathbf{u}|| = 2\sin\theta$. For the purpose of our investigations, the magnitude of rotation was more significant, and so the absolute value of the rotation change was used in SPM.

The first response measurement considered was the *absolute difference* of 3D JSW maps between baseline and follow-up hips as a function of the absolute change in hip rotation. If JSM were significantly dependent on hip rotation, this response would highlight this relation since taking absolute values ensures both an increase and a decrease in the JSW are analogous, thus providing higher statistical power when carrying out SPM. The results of this investigation are illustrated in Figure 21.

The SPM general linear model can be represented as $Y = X\beta + \varepsilon$. The experimental effect (change in hip rotation) forms a column within the design matrix X . The relative contribution of this effect to the observed absolute JSW difference, recorded in the response matrix Y , is measured using least squares regression. β are the regressors or coefficients of linear regression, while ε represents the error (Friston et al. 1994).

A standard two-tail t-test was used to draw inferences about this contribution of hip rotation on the absolute difference in JSW. The t-statistic, in this case, was the GLM coefficient corresponding to hip rotation divided by its standard error (Worsley et al. 2009). Figure 21 shows the mean absolute JSW difference (top). The GLM coefficient corresponding to the hip rotation was also plotted at each vertex of the canonical acetabular surface (middle). These values were small enough such that

¹¹https://en.wikipedia.org/w/index.php?title=Rotation_matrix&oldid=1023582865

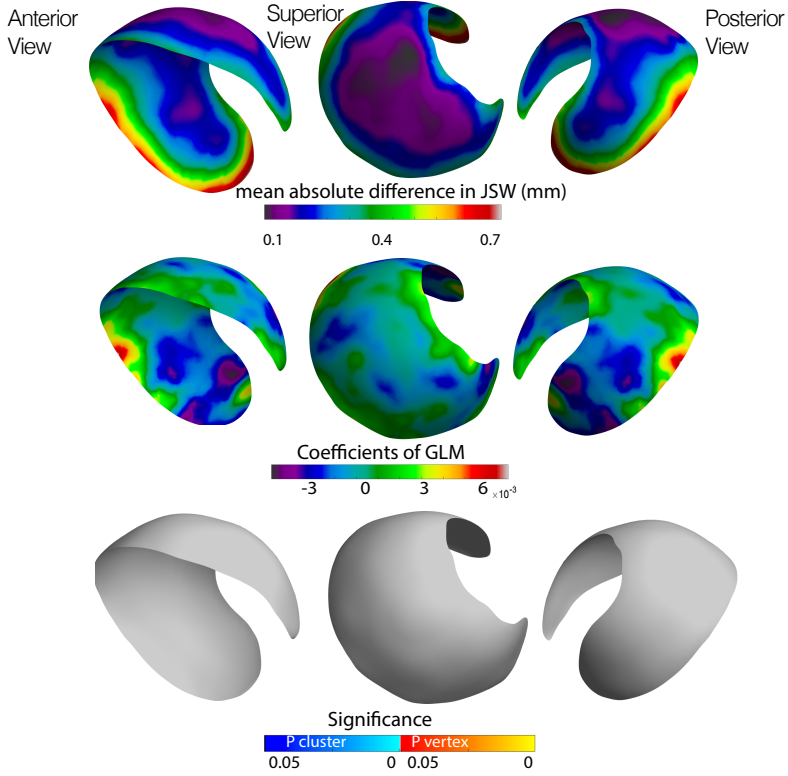


Figure 21: SPM results for the effect of hip rotation difference on the absolute change in 3D JSW. The mean absolute JSW difference (top), coefficients of the SPM general linear model (middle) and p-values at each vertex of the canonical acetabular surface (bottom) are shown.

the p-value at each measurement location was larger than the significance threshold of .05 (bottom), thus indicating that hip rotation had no significant effect on the absolute JSW difference.

It was further hypothesised that the large absolute JSW difference in certain parts of the joint space, particularly around the edges, may be caused by the joint narrowing between the baseline and follow-up scans. However, incorporating the time between scans into the general linear model did not affect the absolute 3D JSW difference. This was mainly because most follow-up scans were carried out within two months of the first one, and this is a short time frame for the joint to significantly degenerate.

These results illustrate that hip rotation has no significant effect on the 3D joint space width output by JSM. The large "error" or absolute difference in JSW at the joint margin may be linked to precision errors that arise due to the multi-staged nature of the JSM pipeline. Previous studies (Turmezei et al. 2018; Turmezei et al. 2020) have shown a global precision of ± 0.32 mm for JSM. This was measured as the standard deviation of the error between JSM and a gold standard HRpQCT approach to measuring joint space width. The largest errors were reported around the

edges of the joint space perimeter. They were caused by a variability in the joint space margin definition between the two methods (Turmezei et al. 2018). The joint space patch segmentation from CT data is error-prone and subject to reproducibility bias, especially around the outer edges, which are harder to discern. An analysis of this precision error was carried out and is discussed in Section 7.6.

7.4 Dependence of Average JSW on Hip Rotation

SPM allows both the magnitude and spatial location of 3D JSW to be incorporated into statistical testing. A more straightforward analysis, investigating the effect of hip rotation on the absolute 3D JSW difference, averaged to a scalar value, was considered next. Averaging would reveal any significant effect of hip rotation on the 3D JSW, regardless of its spatial location.

The scatter plots in Figure 22 show how the mean signed difference (left) and absolute difference (right) in JSW change with hip rotation. The intercept of a linear model fitted to each of these data sets is 0.059 mm for the signed difference, and 0.298 mm for the absolute difference, while the magnitude of regression coefficients is less than 10^{-3} for each. There was no effect of the change in hip rotation on the average signed JSW difference ($P = .49, R^2 = .002$), and the mean was not significantly different from zero ($P = .09$). Furthermore, it was found that there is no significant dependence of the average absolute JSW difference on the change in joint rotation ($P = .94, R^2 = 3 \times 10^{-5}$).

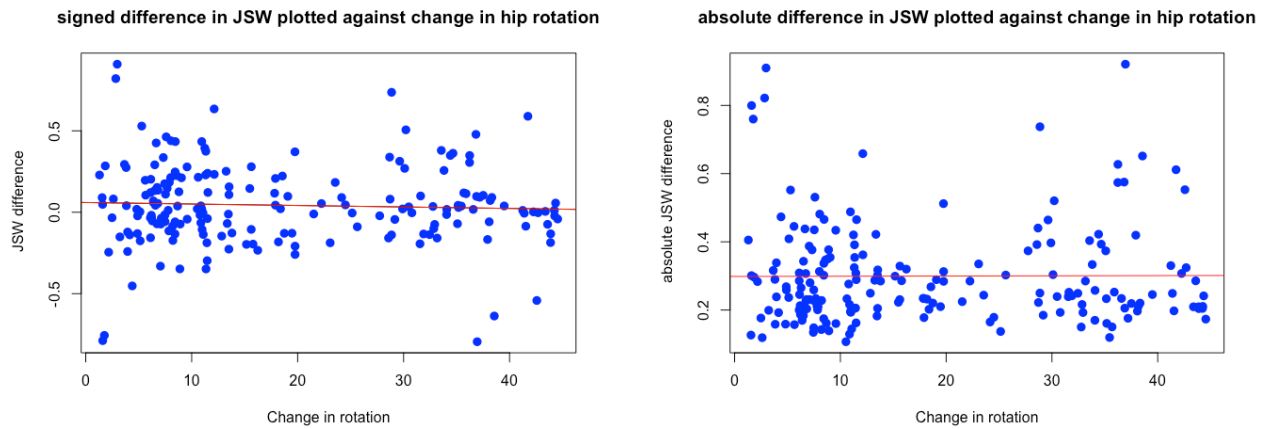


Figure 22: Scatter plots of the signed (left) and absolute (right) 3D JSW difference, averaged to a scalar value, against the absolute change in hip rotation.

The linear model explaining the scatter plot of the absolute JSW difference against hip rotation suggests an agreement with the global precision of ± 0.32 mm reported previously for JSM. As the change in rotation increases, the absolute difference in the joint space width does not deviate

much from the average value of ~ 0.3 mm, less than 10% of the average JSW in a healthy hip joint (Goker et al. 2000). This is considered remarkable for a multi-staged technique, which involves surface registration and data mapping onto a canonical, as well as manual segmentation of both baseline and follow-up acetabular surfaces.

There are outliers in the scatter plot, where regardless of the amount of hip rotation, the average error is large (up to 0.92 mm). As observed in Figure 21, most of this error lies around the outer edge of the acetabular surface. This error may be caused by segmentation differences between the baseline and follow-up joint space patches. Alternatively, the joint may have degraded in these individual cases, leading to a reduction in the JSW between scans.

7.5 Intra-operator Variability of Angle Measurement

The hip rotation measurements have finite precision due to human errors in the angle measurement process. As discussed in Section 5.2, the hip rotation was found by finding the rotation matrix between the femoral and pelvic coordinate systems. Any errors in defining this rotation would be translated into an error in the absolute rotation between baseline and follow-up hips (from Equation 3). Even though we have shown that hip rotation has no apparent effect on the 3D JSW delivered by JSM, high precision in hip angulation measurements will increase our confidence in these statistical results.

The pelvic and femoral coordinate systems were defined by placing landmarks in the CT data and on the mesh objects in *Stradview*. An inherent source of error is the positioning of these landmarks, which will vary within and between operators. For example, the pubic symphysis (see Figure 13) is wide and long, and a landmark placed on its mid-point on the pelvis object would vary between trials. While investigating the inter-operator reproducibility bias of this approach would be more revealing, we were limited by remote work and the lack of volunteers.

Therefore, an intra-operator study was conducted, where the hip rotation was found several times each for a single patient’s baseline and follow-up scans, and the absolute change in hip rotation was calculated according to Equations 3 and 4. The standard deviation between trials was 1.41° when measurements were carried out ten times and averaged to give the final hip rotation difference. The standard deviation was used to calculate the width of the 95% confidence interval. As shown in Figure 23, the width of the 95% confidence interval decreases with the number of trials. For our investigation, carrying out the angle measurements once sufficed. This meant that the true hip rotation difference would have a 95% chance of lying $\pm 2.77^\circ$ around the experimental measurement. The high precision of the semi-automated hip rotation method thus increased our confidence in the outcome of the statistical tests carried out in Sections 7.3 and 7.4, which suggested that hip rotation

is not a significant cause of error in JSM.

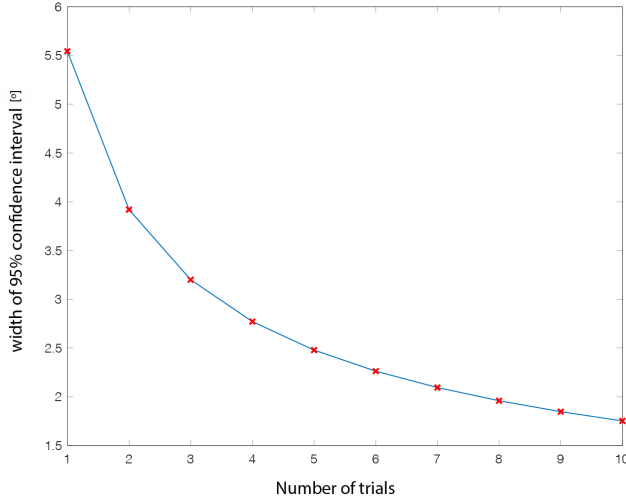


Figure 23: The width of the 95% confidence interval of hip rotation measurements against number of trials.

7.6 Analysis of Joint Space Maps

In order to understand the independence of 3D joint space width and hip rotation, and identify sources of precision error in JSM, *Surfstat* was used to visualise the spatial distribution of joint space width on the canonical acetabular surface. Figure 24 (left) shows the mean 3D JSW for baseline and follow-up scans, as well as the cohort average. The colour bars have identical scales, and it is evident that the mean JSW distribution does not change much between the baseline and follow-up hips. The mean spatial distribution of JSW in this cohort strongly agrees with that of healthy hips used as a control group in the study conducted by Turmezei et al. (2020), which explored the effects of future total hip replacement on 3D joint space width. The posterior joint space is narrowest at ~ 2.5 mm while the superior and anterior joint regions are wider at ~ 4 mm.

There is a slightly more pronounced JSW at the superior edge of the joint for the baseline scans, which could arise from a slight narrowing of the joint space for some patients between scans. However, the interval between repeat scans had no significant effect on the absolute difference in JSW when it was included in the SPM general linear model.

The other likely cause of the precision error of JSM is the difference in the joint patches segmented out for the baseline and follow-up hips. Segmentation effects could result in patches that differ in size or shape. When JSM is run on a larger patch, data from further out in the joint is mapped onto its vertices, compared to a smaller patch. This can lead to an inconsistent spatial distribution of the JSW between the baseline and follow-up patches, which, after spatial normalisation, manifests as

JSW differences around the outer edges of the canonical acetabular surface.

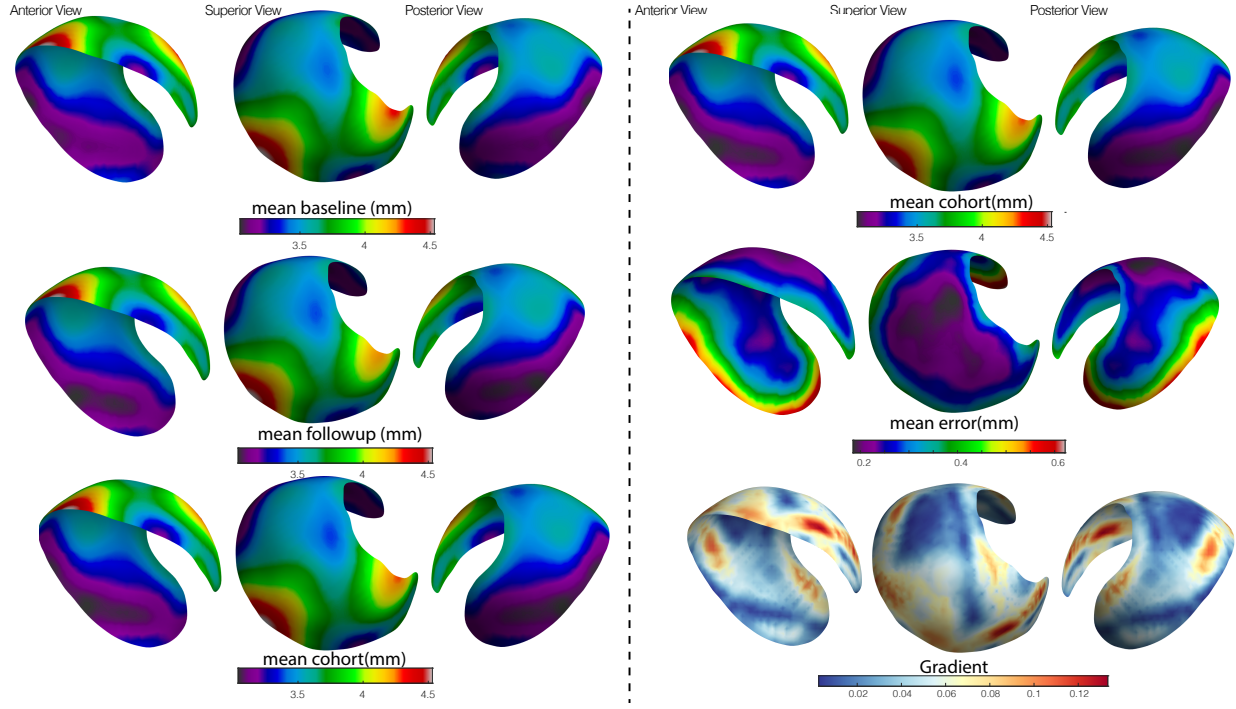


Figure 24: Analysis of joint space maps.

One way to check whether segmentation effects cause high errors around the outer edge of the joint space is to plot the gradient of the cohort average JSW data around the canonical acetabular surface. Areas of high gradient correspond to regions where the joint space changes rapidly. Therefore, even minute segmentation errors would be significantly pronounced in these regions. This is because inconsistent JSW data would be mapped from the baseline and follow-up patches onto the canonical, resulting in errors.

The gradient of the cohort average JSW was calculated at each vertex of the canonical acetabular surface. Details of the mesh topology, such as the coordinates of each vertex and a list of vertices forming each edge, were extracted from the mesh's VRML file using MATLAB. The gradient was calculated at each edge as the ratio of the absolute difference in data value at the two vertices forming the edge to the edge length. The gradient values at edges connected to a vertex were then averaged to find the value of the gradient at the vertex.

Figure 24 (right) shows the average cohort JSW distribution (top), the spatial distribution of the error between baseline and follow-up JSW measurements (middle) and the spatial gradient of the mean JSW distribution (bottom). The JSW gradient is prominent around the superior margin, which corresponds to a larger error compared to regions away from the edges. Similarly, in the posterior

view, certain areas of high gradient map to high errors. However, the gradient map cannot explain some regions of the joint space with large errors, particularly at the posteroinferior edge of the joint. This is a reportedly challenging region to segment out (Turmezei et al. 2018), and thus, the standard deviation in the joint space perimeter demarcated in this region is large both within and between observers. This causes the error to be large here, despite a moderate gradient.

As described in Section 1.3.1, the perimeter of the joint space is cut out as the shadow of the acetabulum on the proximal femur. This shadow is found by projecting the highest CT data value sampled through the 3D image data volume, within a distance L along the normal to each vertex of the proximal femur mesh, back onto the femur mesh. The length L of this normal, referred to as the compounding depth, controls the size of the joint space perimeter.

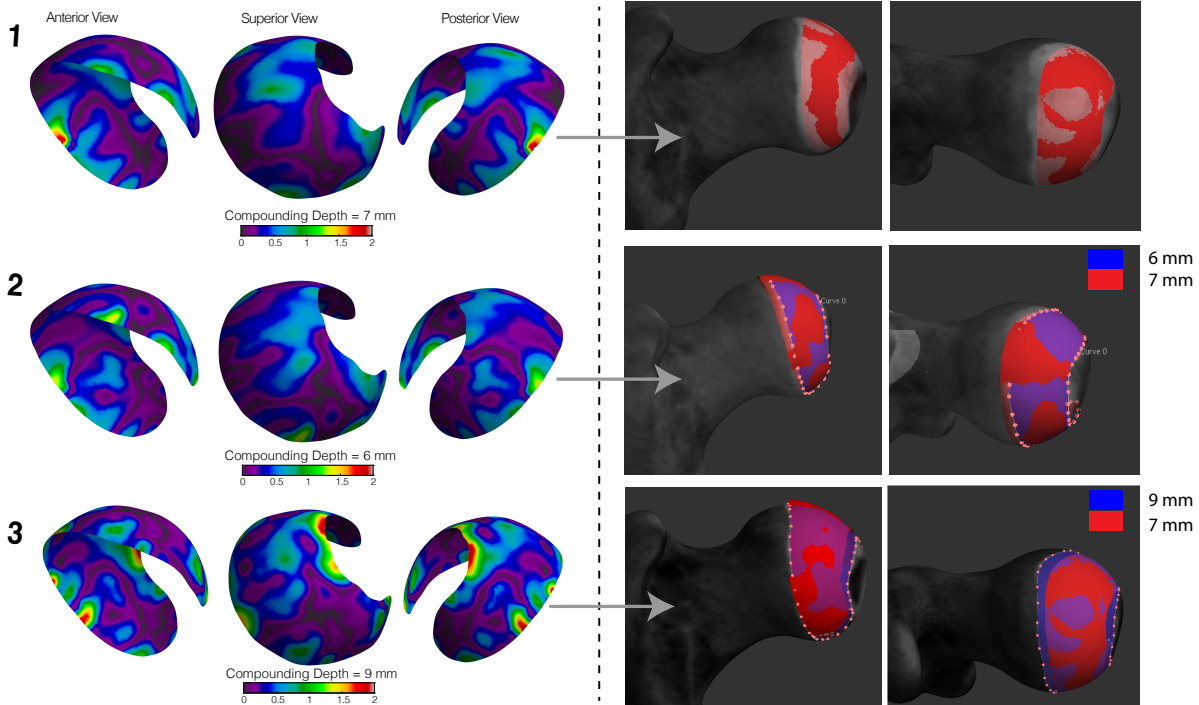


Figure 25: Effect of compounding depth on the baseline follow-up error.

1. Using a compounding depth of 7 mm resulted in an average error of 0.40 mm across the joint space, with a large error around the perimeter.
2. A compounding depth of 6 mm reduced the joint space patch size. The average error also reduced to 0.34 mm. There was a noticeably reduced error around the outer edges.
3. An increased compounding depth increased the extent of the projected shadow, especially towards the fovea of the proximal femur. The average error increased to 0.44 mm, with a noticeably larger error on the joint space edge closest to the fovea.

For this project, the acetabular surface for each hip was segmented out by an expert radiologist

who used a fixed compounding depth of 7 mm. As the proximal femur rotates, the position of normals at each vertex changes, and thus the shadow of the opposing acetabular surface projected onto the proximal femur mesh changes between baseline and follow-up hips. We carried out an exploratory study into the effect of the perimeter size of the follow-up joint space patch, affected by the value of L , on the absolute difference between the baseline and follow-up JSW. A hip with a moderate average JSW error of 0.4 mm was selected, and the follow-up patch was segmented at three different compounding depths. The result of this investigation is shown in Figure 25.

Another possible approach is to use the same joint space patch to map data from both the baseline and follow-up hips to improve precision. Therefore, the patch was extracted according to Figure 2 for the baseline hip. This joint space patch was saved as a template mesh and fitted to the follow-up hip using *Stradview*'s model fitting functionality. A joint space outline was manually drawn, and the template mesh was fitted using a rigid deformation, allowing for scaling, translation and rotation. Data sampling was then carried out on these joint space patches as usual.

The process described above was carried out for a subset of 10 baseline follow-up hip pairs. The average absolute JSW difference was found and recorded. Figure 26 shows the results of this investigation. While it was initially hypothesised that using the same joint space patch for both the initial and repeat scans of each hip might improve the test-retest precision of JSM, we discovered that this exacerbated segmentation effects, particularly at the posterior joint space.

From our analyses, it is evident that it is good practice to re-segment the joint space patches for repeat scans since this improves the precision of JSM. However, the joint space perimeter location has a considerable effect on the measurements reported around the edges due to a large JSW gradient here. Therefore, choosing the right compounding depth is critical since this affects the joint space margin. While the results of Figure 25 show that a smaller compounding depth reduced the overall error, in another individual's hip, a larger compounding depth of 9 mm proved optimal. Perhaps a sensible approach to improving JSM precision is to repeat the patch extraction process a few times and finding the average patch shape. Alternatively, a statistical shape model for the joint space patch could be trained on a large patient dataset to capture the principal modes of shape variation. This could subsequently be used to segment anatomically plausible joint space patches, with appropriate user intervention where necessary.

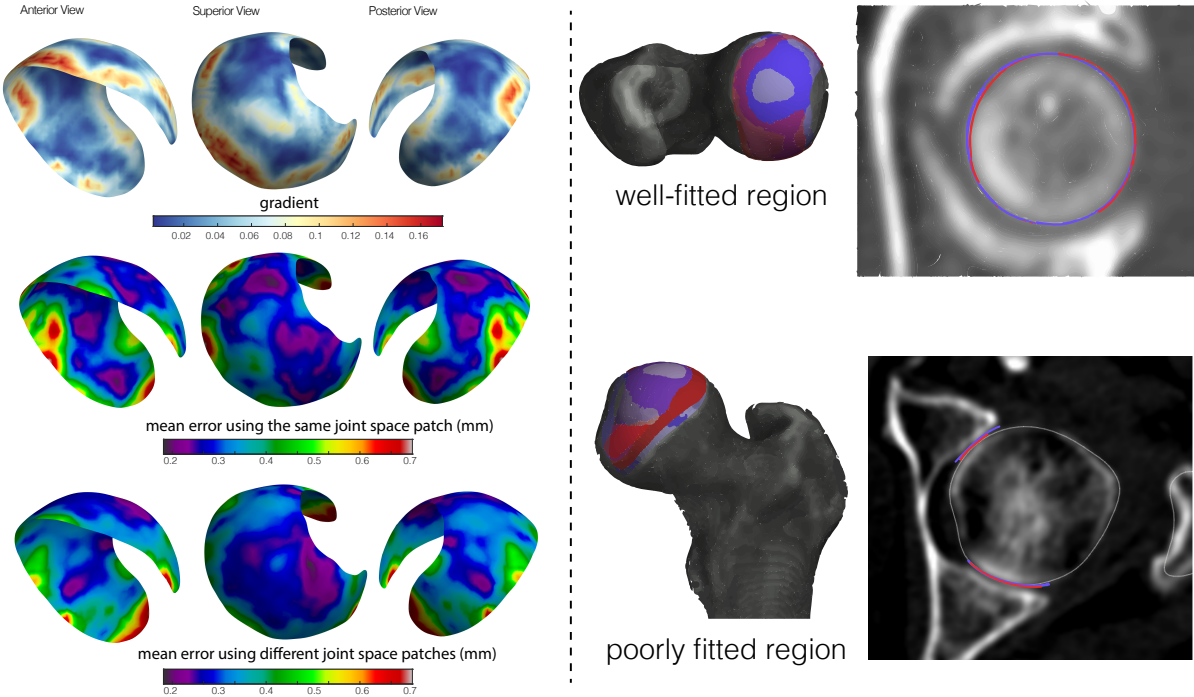


Figure 26: Effect of using the same joint space patch for baseline and follow-up data sampling.

(Left) The error averaged over the entire joint space increased to 0.29 mm, from 0.26 mm previously, when the same patch for mapping both joints’ data was used. The gradient of the average joint space width is high around the outer edge of the joint space, with a correspondence between areas of high error and high gradient.

(Right) The errors in segmentation when the **baseline acetabular mesh** is fit to the **follow-up acetabular shadow** using rigid body transformations only. The poor fit around the outer edge of the posterior joint space corresponds to a high error, suggesting that segmentation effects may lead to a precision error in joint space mapping.

7.7 Stratification of Data

In order to further understand the effect of hip rotation on 3D joint space width, the patients were grouped according to the magnitude of hip rotation between baseline and follow-up scans. Two subgroups were created such that group 1 included patients whose hips rotated less than 20° and group 2 included patients that rotated their hips by more than 20° . This stratification study aimed to isolate regions of the joint space that differ significantly between the two groups and determine if the average absolute error in JSW depended on the patient group.

Figure 27 shows the results of this investigation. The colour bars have identical scales, indicating that the gradient around the patch’s margin is larger for group 2. This, in turn, corresponds to a

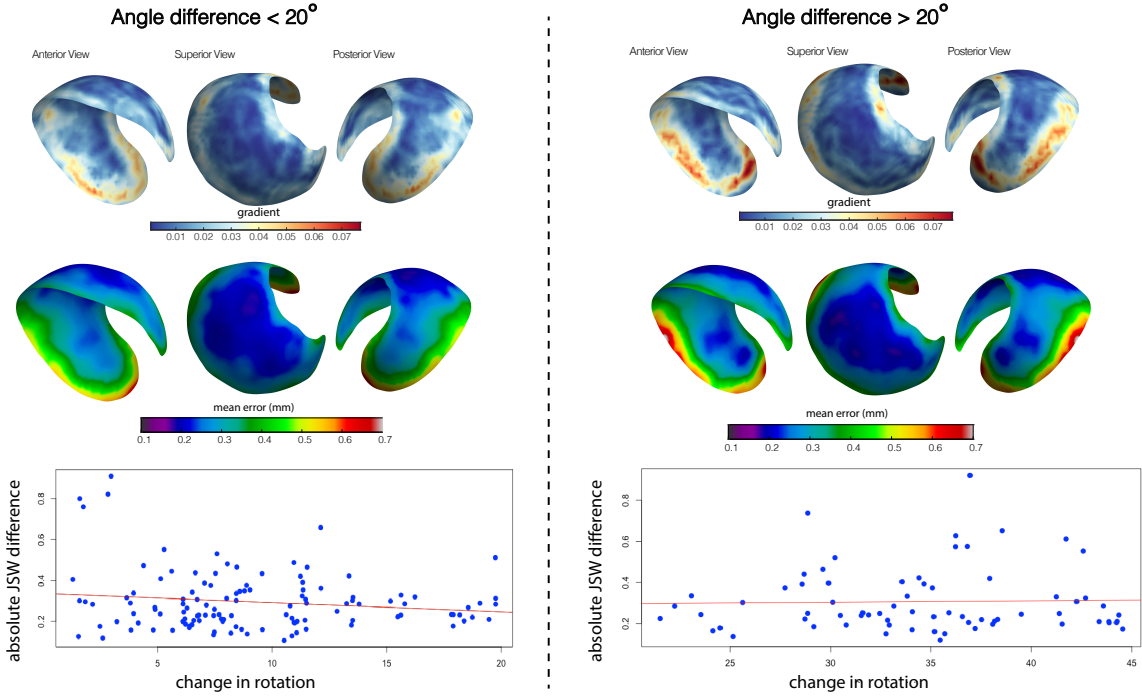


Figure 27: Stratification of hips into two groups. While the error at the joint space margin was larger for hips with larger rotation between scans, there was not enough evidence to suggest a significant effect of group type (small vs large angulation) on the absolute 3D JSW difference.

larger error in the joint space width distribution between baseline and follow-up, suggesting that segmentation effects have a higher impact on group 2. SPM was carried out to determine the effect that group type had on the error, measured as the absolute difference in the baseline and follow-up JSW. However, this revealed no regional effects of group type on the mean error ($P > .05$ at each vertex).

A two-sample t-test was also carried out to compare the mean error for group 1 ($M = 0.294$ mm, $SD = 0.11$ mm), obtained by averaging the mean JSW over each vertex of the joint space patch, with the mean error for group 2 ($M = 0.321$ mm, $SD = 0.15$ mm). This revealed no significant effect of group type, and thus the amount of hip rotation, on the mean error ($P = .61$). A scatter plot of the vertex averaged JSW for each patient against the hip rotation is shown in Figure 27 (bottom). The magnitude of regression coefficients was less than 10^{-3} for both groups, and two-tailed t-testing revealed that there was no effect of the change in hip rotation on the average absolute JSW difference for either group ($P > .05$).

7.8 Reproducibility Bias of JSM

In one study, Turmezei et al. (2018) have shown that JSM has a minimal inter-operator reproducibility bias, with a mean of -0.03 mm and limits of agreement ± 0.40 mm. The limits of agreement were calculated as $1.96 \times$ standard deviation of the bias. The largest reproducibility error occurs around the joint space margin and has been reported to be an effect of the variability between users in the joint space margin definition (Figure 28, left).

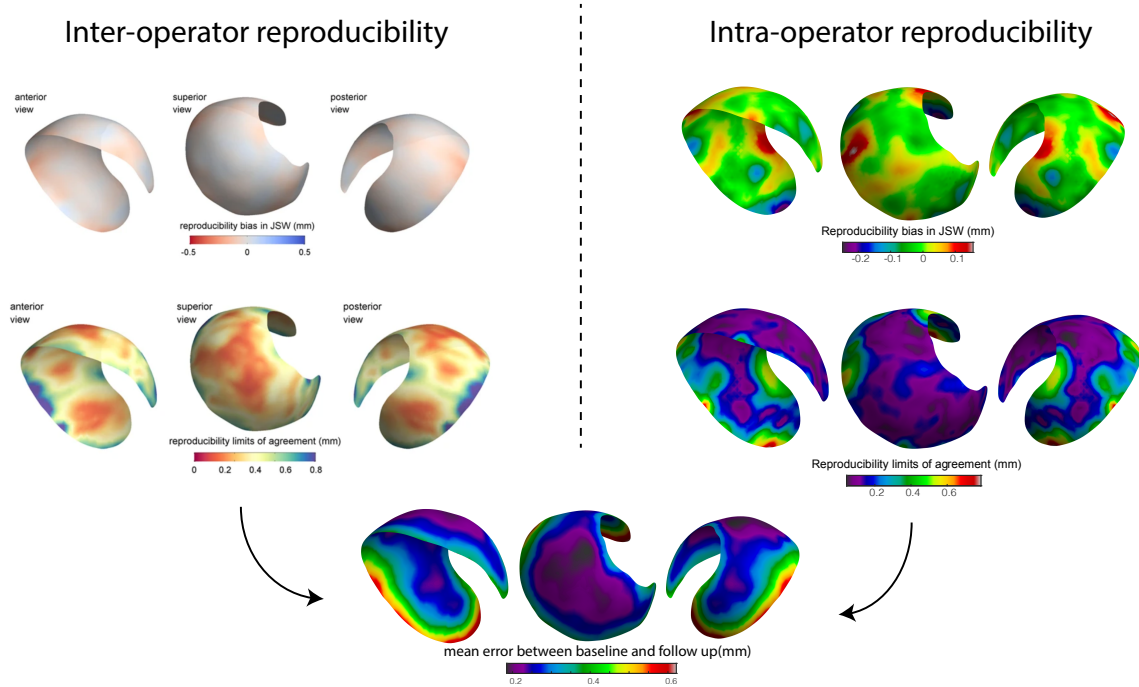


Figure 28: Reproducibility bias of JSM compared to the mean absolute JSW difference between baseline and follow up hips. Both intra and inter-operator reproducibility worsen at the outer edge of the joint, consistently with the mean error found in our study. This strongly suggests that segmentation effects lead to a degraded precision around the margin ¹².

An expert radiologist carried out all joint space patch segmentations for this project, thus removing the inter-operator bias. However, since JSM is highly sensitive to segmentation errors, especially around regions of high JSW gradient, the intra-operator reproducibility bias was also investigated. JSM was carried out on ten hips twice by a single operator, and the mean bias and limits of agreement were calculated. These are reported in Figure 28 (right).

These results indicate that even when the same operator carries out JSM, segmentation artefacts lead to large measurement noise. This noise masks the effect, if any, of hip rotation on the absolute

¹² Adapted Turmezei et al. (2018) Figure 4.

JSW difference. This is especially true if the effect is already minimal.

7.9 Limitations

This project has investigated the effect of hip angulation on JSM and shown that the method is robust to hip positioning during CT acquisition. However, there are a few limitations to the investigation that should be addressed in future work that may be carried out in this area.

1. Spatial normalisation, which involves aligning each individual's acetabular surface to the canonical, may be affected by misregistration. This misregistration generally depends on the shape of the specimens and can result in a systematic bias that might alter the significance of statistical tests carried out. This can be circumvented by allowing for shape as a confounding factor in the SPM general linear model (Gee et al. 2014). This has been shown to reveal true effects that could previously be masked by systematic misregistration. While there was no significant effect of hip rotation found on 3D JSW, the effect may be too small compared to a potential systematic misregistration bias, thus masking any significance. Accounting for the shape, represented by the dominant modes of variation observed in the cohort, may help pronounce the effect of angulation on JSM more.
2. None of the patients in this study had a standardised hip positioning. There is a possibility of the effect of hip angulation on JSM being small and thus concealed by measurement noise. Therefore, having a control group of patients, whose hip position was standardised by strapping their knees together (Turmezei et al. 2020), might serve as a useful baseline to compare our results against. Standardisation of hip positioning could be input into the SPM general linear model as a boolean variable to increase statistical power. Having a control group would reduce confirmation bias and potentially reveal the effects of hip rotation on 3D JSW despite measurement noise. This is because the presence of a control group could correct for the systematic user bias, if any, in the joint space patch segmentation process.
3. The femoral neck axis significantly deviates from our current definition in patients suffering from femoroacetabular impingement (Davda et al. 2011). Our semi-automated method of finding the hip rotation relied on none of the patients having this condition. If this method were to be used to find clinically-relevant joint angles or obtain the matrix for hip rotation, a more consistent definition of the femoral coordinate system might need to be used, which works well with individuals with and without femoroacetabular impingement.

8 Summary and Recommendations for Further Study

8.1 Conclusions

This project has analysed the sensitivity of JSM to hip positioning and has investigated the importance of consistent joint positioning for retrospective analyses of joint space maps.

In order to obtain a metric for the hip joint rotation, a semi-automated angulation protocol was devised. This relied on manipulating triangulated meshes of the pelvis and the proximal femur to yield a rotation matrix that quantified the hip joint rotation. The semi-automated protocol additionally allowed us to extract anatomically plausible hip rotation measurements and compare them with those acquired manually by clinicians.

Secondly, the effect of hip rotation on JSM was investigated. We found no significant evidence that a change in hip rotation affects the absolute JSW difference between baseline and follow-up measurements. We concluded that hip angulation was not a significant source of error in the JSM workflow, which had a test-retest precision of ~ 0.3 mm. This precision is in agreement with that previously reported for JSM (Turmezei et al. 2018). This result provides confidence in all subsequent retrospective analyses of joint space maps wherein patient positioning was not standardised.

Finally, sources of precision error in the JSM pipeline were investigated. We found that the error, reported as the absolute difference between the baseline and follow-up JSW, was caused, in part, by a reproducibility bias in the segmentation of the joint space patch. The error was more pronounced around the joint space margin and, due to a high JSW gradient in this region, was very sensitive to the compounding depth (and hence the joint space patch size).

In summary, this project has shown that JSM is robust to changes in hip rotation. Any measurement noise induced by inconsistent hip positioning is insignificant compared to other sources of error and does not worsen the already established precision of the technique.

8.2 Recommendation for Future Work

In order to disentangle measurement noise from any possible effects of hip rotation on JSM, a study involving both a control group and an experimental group could be carried out. The control group would have standardised hip positioning between scans by, for example, having their feet strapped together. The experimental group would not have a standardised hip position. Additionally, the most prominent shape modes of the subject acetabular surfaces could be included in the SPM general linear model as confounding variables. Such a study would be more sensitive to any effects of

hip rotation on the 3D JSW. This is because the control group could correct for any systematic user bias in the JSM workflow, while the incorporation of shape modes would remove any systematic misregistration bias that may affect the significance of results.

Furthermore, a straightforward way of standardising the joint space patch segmentation could use a statistical shape model of the patch, trained on a large dataset. This could be fit to the joint space outline in *Stradview* using SSM registration, which would only allow anatomically plausible joint space patch definitions, potentially reducing segmentation errors in the JSM workflow. Further investigation into the effects of using a statistical shape model on the precision of JSM is therefore recommended.

A Impact of COVID-19

COVID-19 did not affect the goals or outcome of this project significantly. The only impact was that inter-observer variation could not be measured in the hip angulation protocol devised in the project due to remote working and a lack of available volunteers. The project was entirely computational, and no laboratory access was required. Therefore, no data collection was compromised, and the key objectives and approaches did not need to be modified.

B Risk assessment retrospective

This project was entirely computational and, as such, relatively low-risk. In hindsight, the risk assessment submitted was appropriate for this project. The main risks stemmed from the workspace set-up and involved prolonged computer usage, which could lead to repetitive strain injury. By ensuring that the display screen equipment was set up appropriately, and taking regular breaks, most of these risks were mitigated.

References

- Bonneau, N. et al. (Nov. 2012). “A three-dimensional axis for the study of femoral neck orientation”. In: *Journal of anatomy* 221.5, pp. 465–476. ISSN: 1469-7580. DOI: [10.1111/j.1469-7580.2012.01565.x](https://doi.org/10.1111/j.1469-7580.2012.01565.x). URL: <https://pubmed.ncbi.nlm.nih.gov/22967192/>.
- Cappozzo, A. et al. (1995). “Position and orientation in space of bones during movement: anatomical frame definition and determination”. In: *Clinical Biomechanics* 10.4, pp. 171–178.
- Davda, K. et al. (2011). “The 3D femoral neck axis- a novel method to explore the had-neck relationship in normal and cam hips”. In: *Orthopaedic Proceedings* 93-B, pp. 388–388.
- Felson, D. T. (Mar. 1988). “Epidemiology of hip and knee osteoarthritis”. In: *Epidemiologic Reviews* 10.1, pp. 1–28. ISSN: 0193-936X.
- Fischer, M. C. M. et al. (Nov. 2020). “A robust method for automatic identification of femoral landmarks, axes, planes and bone coordinate systems using surface models”. In: *Scientific Reports* 10.1, p. 20859. ISSN: 2045-2322. DOI: [10.1038/s41598-020-77479-z](https://doi.org/10.1038/s41598-020-77479-z). URL: <https://doi.org/10.1038/s41598-020-77479-z>.
- Friston, K. J. et al. (1994). “Statistical parametric maps in functional imaging: A general linear approach”. In: *Human Brain Mapping* 2.4, pp. 189–210.
- Gee, A. H. and G. M. Treece (2014). “Systematic misregistration and the statistical analysis of surface data”. In: *Medical Image Analysis* 18.2, pp. 385–393. ISSN: 1361-8415. DOI: <https://doi.org/10.1016/j.media.2013.12.007>. URL: <https://www.sciencedirect.com/science/article/pii/S1361841513001783>.
- Goker, B. et al. (2000). “Quantification of progressive joint space narrowing in osteoarthritis of the hip: Longitudinal analysis of the contralateral hip after total hip arthroplasty”. In: *Arthritis & Rheumatism* 43.5, pp. 988–994.
- Goker, B. et al. (2005). “The effects of minor hip flexion, abduction or adduction and x-ray beam angle on the radiographic joint space width of the hip”. In: *Osteoarthritis and Cartilage* 13.5, pp. 379–386. ISSN: 1063-4584.
- Goodall, C. (1991). “Procrustes Methods in the Statistical Analysis of Shape”. In: *Journal of the Royal Statistical Society. Series B (Methodological)* 53.2, pp. 285–339. ISSN: 00359246. URL: <http://www.jstor.org/stable/2345744>.
- Gunz, P. and P. Mitteroecker (2013). “Semilandmarks: a method for quantifying curves and surfaces”. In: *Hystrix, the Italian Journal of Mammalogy* 24.1, pp. 103–109. ISSN: 0394-1914.
- Gunz, P., P. Mitteroecker, and F. Bookstein (Jan. 2005). “Semilandmarks in Three Dimensions”. In: *Modern Morphometrics in Physical Anthropology*. Springer US, pp. 73–98. ISBN: 0-306-48697-0. DOI: [10.1007/0-387-27614-9_3](https://doi.org/10.1007/0-387-27614-9_3).
- Hartel, M. J. et al. (2016). “Determination of Femoral Neck Angle and Torsion Angle Utilizing a Novel Three-Dimensional Modeling and Analytical Technology Based on CT Datasets”. In: *PLOS ONE* 11.3, pp. 1–10. DOI: [10.1371/journal.pone.0149480](https://doi.org/10.1371/journal.pone.0149480). URL: <https://doi.org/10.1371/journal.pone.0149480>.
- Hunter, D. J. et al. (2015). “OARSI Clinical Trials Recommendations: Knee imaging in clinical trials in osteoarthritis”. In: *Osteoarthritis and Cartilage* 23.5, pp. 698–715.
- Kang, Y. et al. (Oct. 2005). “An anatomic coordinate system of the femoral neck for highly reproducible BMD measurements using 3D QCT”. In: *Computerized Medical Imaging and Graphics*

- 29.7, pp. 533–541. ISSN: 0895-6111. DOI: [10.1016/j.compmedimag.2005.05.002](https://doi.org/10.1016/j.compmedimag.2005.05.002). URL: <https://www.sciencedirect.com/science/article/pii/S089561105000637>.
- Kellgren, J. H. and J. S. Lawrence (Dec. 1957). “Radiological assessment of osteo-arthrosis”. In: *Annals of the rheumatic diseases* 16.4, pp. 494–502.
- Lindberg, H. and F. Montgomery (Jan. 1987). “Heavy labor and the occurrence of gonarthrosis”. In: *Clinical Orthopaedics and Related Research* 214, pp. 235–236. ISSN: 0009-921X.
- Mannava, S. et al. (2017). “Comprehensive Clinical Evaluation of Femoroacetabular Impingement: Part 2, Plain Radiography”. In: *Arthroscopy Techniques* 6.5, e2003–e2009. ISSN: 2212-6287. DOI: <https://doi.org/10.1016/j.eats.2017.06.011>. URL: <https://www.sciencedirect.com/science/article/pii/S2212628717301767>.
- Murray-Leslie, C. F., D. J. Lintott, and V. Wright (Aug. 1977). “The knees and ankles in sport and veteran military parachutists”. In: *Annals of the rheumatic diseases* 36.4, pp. 327–331. ISSN: 0003-4967. DOI: [10.1136/ard.36.4.327](https://doi.org/10.1136/ard.36.4.327). PMID: 409358. URL: <https://pubmed.ncbi.nlm.nih.gov/409358>.
- Ornetti, P. et al. (July 2009). “OARSI-OMERACT definition of relevant radiological progression in hip/knee osteoarthritis”. In: *Osteoarthritis and cartilage* 17.7, pp. 856–863.
- Polesello, G. C. et al. (2011). “Proposal for standardisation of radiographic studies on the hip and pelvis”. In: *Revista Brasileira de Ortopedia (English Edition)* 46.6, pp. 634–642. ISSN: 2255-4971. DOI: [https://doi.org/10.1016/S2255-4971\(15\)30318-9](https://doi.org/10.1016/S2255-4971(15)30318-9). URL: <https://www.sciencedirect.com/science/article/pii/S2255497115303189>.
- Poole, K. E. et al. (2017). “Focal osteoporosis defects play a key role in hip fracture”. In: *Bone* 94, pp. 124–134. ISSN: 8756-3282. DOI: <https://doi.org/10.1016/j.bone.2016.10.020>. URL: <https://www.sciencedirect.com/science/article/pii/S8756328216303167>.
- Tom, S. et al. (Oct. 2016). “Determining Metacarpophalangeal Flexion Angle Tolerance for Reliable Volumetric Joint Space Measurements by High-resolution Peripheral Quantitative Computed Tomography”. In: *The Journal of Rheumatology* 43, pp. 1941–1944.
- Treece, G. M. and A. H. Gee (2015a). “Independent measurement of femoral cortical thickness and cortical bone density using clinical CT”. In: *Medical Image Analysis* 20.1, pp. 249–264.
- Treece, G. M., K. E. S. Poole, and A. H. Gee (2012). “Imaging the femoral cortex: Thickness, density and mass from clinical CT”. In: *Medical Image Analysis* 16.5, pp. 952–965.
- Treece, G. M., R. W. Prager, and A. H. Gee (1998). “Regularised Marching Tetrahedra: Improved Iso-Surface Extraction”. In: *Computers and Graphics* 23, pp. 583–598.
- Treece, G. M. et al. (2010). “High resolution cortical bone thickness measurement from clinical CT data”. In: *Medical Image Analysis* 14.3, pp. 276–290.
- Treece, G. M. et al. (Nov. 2015b). “Predicting Hip Fracture Type With Cortical Bone Mapping (CBM) in the Osteoporotic Fractures in Men (MrOS) Study”. In: *Journal of bone and mineral research : the official journal of the American Society for Bone and Mineral Research* 30.11, pp. 2067–2077.
- Turmezei, T. D. et al. (2014). “A new CT grading system for hip osteoarthritis”. In: *Osteoarthritis and Cartilage* 22.10, pp. 1360–1366.
- Turmezei, T. D. et al. (2016). “3D modelling of the hip joint from clinical imaging data”. In: *Osteoarthritis and Cartilage* 24, S293–S294.

- Turmezei, T. D. et al. (2018). “A new quantitative 3D approach to imaging of structural joint disease”. In: *Scientific Reports* 8.1, p. 9280.
- Turmezei, T. D. et al. (2020). “Quantitative 3D imaging parameters improve prediction of hip osteoarthritis outcome”. In: *Scientific Reports* 10.1, p. 4127.
- Whitmarsh, T. et al. (2017). “An exploratory study into measuring the cortical bone thickness from CT in the presence of metal implants”. In: *International Journal of Computer Assisted Radiology and Surgery* 12.12, pp. 2079–2086.
- Worsley, K. et al. (July 2009). “SurfStat: A Matlab toolbox for the statistical analysis of univariate and multivariate surface and volumetric data using linear mixed effects models and random field theory”. In: *NeuroImage* 47, S102. ISSN: 10538119. DOI: [10.1016/S1053-8119\(09\)70882-1](https://doi.org/10.1016/S1053-8119(09)70882-1). URL: <https://linkinghub.elsevier.com/retrieve/pii/S1053811909708821> (visited on 03/12/2021).
- Wu, G. et al. (2002). “ISB recommendation on definitions of joint coordinate system of various joints for the reporting of human joint motion—part I: ankle, hip, and spine”. In: *Journal of Biomechanics* 35.4, pp. 543–548. ISSN: 0021-9290. DOI: [https://doi.org/10.1016/S0021-9290\(01\)00222-6](https://doi.org/10.1016/S0021-9290(01)00222-6). URL: <https://www.sciencedirect.com/science/article/pii/S0021929001002226>.
- Zhang, R.-Y. et al. (May 2020). “Three-dimensional morphological analysis of the femoral neck torsion angle—an anatomical study”. In: *Journal of Orthopaedic Surgery and Research* 15.1, p. 192. ISSN: 1749-799X. DOI: [10.1186/s13018-020-01712-8](https://doi.org/10.1186/s13018-020-01712-8). URL: <https://doi.org/10.1186/s13018-020-01712-8>.